Journal of Computational Physics 528 (2025) 113844

Contents lists available at ScienceDirect

Journal of Computational Physics

journal homepage: www.elsevier.com/locate/jcp

A new boundary condition for the nonlinear Poisson-Boltzmann equation in electrostatic analysis of proteins

Sylvia Amihere [a], Yiming Ren [a], Weihua Geng [b], Shan Zhao [a,*]

[a] Department of Mathematics, University of Alabama, Tuscaloosa, AL 35487, USA
[b] Department of Mathematics, Southern Methodist University, Dallas, TX 75275, USA

ARTICLE INFO

Dataset link: https://www.rcsb.org

Keywords:
Nonlinear Poisson-Boltzmann equation
Elliptic interface problem
Modified Robin boundary condition
Electrostatic analysis
Kirkwood sphere
Matched Interface and Boundary (MIB) method

ABSTRACT

As a well-established implicit solvent model, the Poisson-Boltzmann equation (PBE) models the electrostatic interactions between a solute biomolecule and its surrounding solvent environment over an unbounded domain. One numerical challenge in solving the nonlinear PBE lies in the boundary treatment. Physically, the boundary condition of this solute solvent system is defined at infinity where the electrostatic potential decays to zero. Computationally, a finite domain has to be employed in grid-based numerical algorithms. However, the Dirichlet boundary conditions commonly used in protein simulations are known to produce unphysical solutions in some cases. This motivates the development of a few asymptotic conditions in the PBE literature, which are global boundary conditions and have to resort to iterative algorithms for calculating volume integrals from the previous step. To overcome these limitations, a modified Robin condition is proposed in this work as a local boundary condition for the nonlinear PBE, which can be implemented in any finite difference or finite element method. The derivation is based on the facts that away from the biomolecule, the asymptotic decaying pattern of the nonlinear PBE is essentially the same as that of the linearized PBE, and the monopole term will dominate other terms in the multipole expansion. Asymptotic analysis has been carried out to validate the application range and robustness of the proposed Robin condition. Moreover, a second order boundary implementation by means of a matched interface and boundary (MIB) scheme has been constructed for three-dimensional biomolecular simulations. Extensive numerical experiments have been conducted to examine the robustness, accuracy, and efficiency of the new boundary treatment for calculating electrostatic free energies of Kirkwood spheres and various protein systems.

1. Introduction

Electrostatic analysis of biomolecules immersed in a solvent environment with dissolved electrolytes plays an important role in understanding the structure, function and behavior of macromolecules such as proteins, DNAs and RNAs. One of the most widely used implicit solvent models for the electrostatic analysis of proteins is the Poisson-Boltzmann Equation (PBE) [2,13,20,22]. In the Poisson-Boltzmann (PB) model, the solute biomolecule is treated as a low-dielectric medium with atomic partial charges, surrounded by a high-dielectric medium of the solvent with dissolved ions. The PB model has found applications in various biological and

* Corresponding author.
E-mail address: szhao@ua.edu (S. Zhao).

https://doi.org/10.1016/j.jcp.2025.113844
Received 5 June 2024; Received in revised form 28 November 2024; Accepted 10 February 2025

Available online 13 February 2025

chemical processes such as DNA recognition [11], drug development and design, protein folding [31], and the designing of nanoscale semiconductor devices [39].

Mathematically, the PBE is a nonlinear elliptic partial differential equation (PDE) with singular source terms and defined over solute and solvent subdomains separated by a molecular surface. The analytical solution of the PBE is limited to simple geometries such as a sphere [1] or in one dimensional planar case [35], so that numerical simulations are indispensable for electrostatic analysis of protein systems containing tens of thousands to millions of atoms. However, the numerical solution of the PBE in three dimensions (3D) suffers many challenges such as (1) the potential is infinity at atomic centers due to point sources modeled with delta functions; (2) the molecular surface is a geometrically complicated solute-solvent boundary; (3) the dielectric function and electric field are discontinuous across the molecular surface; (4) the hyperbolic Sine term could introduce a nonlinear instability; (5) the domain is unbounded.

Physically, the PB model involves an unbounded solvent domain with the electrostatic potential decaying to zero at infinity, i.e., $\lim_{|\mathbf{r}|\to\infty} u(\mathbf{r}) = 0$. In the PBE literature, the numerical treatments of the infinite domain fall into two classes. First, the infinite domain problem can be simply bypassed when solving the linearized PBE in an integral form, in which surface integral equations need to be evaluated over two-dimensional (2D) molecular surfaces, and can be discretized by various boundary element methods [7,16,28,41,45]. Moreover, the singular charges and interface jump conditions can also be treated analytically in boundary element methods. However, these integral equation methods work only for the linearized PBE, and cannot handle the nonlinear PBE. Second, in grid-based finite difference and finite element methods [4,9,10,22,29,36,42], the infinite domain has to be truncated to a finite computational domain Ω and an appropriate boundary condition is then required on the boundary $\partial\Omega$. The formulation of the boundary condition is a critical issue here to guarantee that the numerical solution over the truncated domain could be a reliable approximation to the original infinite domain problem.

Theoretically, a Dirichlet boundary condition with potential equaling to zero could be assumed when a very large truncation domain is used, because the electrostatic potential decays exponentially away from the solute biomolecule. Nevertheless, for real protein simulations, the dimension of biomolecules is already very large, so that a small edge value, which determines the distance between the molecular surface and the boundary, is often preferred. In such scenarios, the most widely used boundary condition in the PBE literature is a Debye-Hückel Dirichlet condition [20], which is obtained from an analytical solution of the linearized PBE under the assumption that the solvent is fully penetrating to the entire domain and each atom is treated as one point charge. As explained in [20], this analytical solution is derived based on the Kirkwood sphere solution by taking the radius as zero and applying the superposition principle to all point charges. Alternatively, by applying the superposition principle to Kirkwood sphere solutions with nonzero radii, a multiple Debye-Hückel (MDH) Dirichlet boundary condition can be obtained [3], which is essentially an approximated solution of the linearized PBE far away from the protein. These Dirichlet boundary conditions are widely used in various PBE solvers in the literature [4,9,10,17–19,26,36].

However, the application of Dirichlet boundary conditions derived from the linearized PBE to the nonlinear PBE can be problematic. Recently, the electrostatic free energy governed by the nonlinear PBE for the Kirkwood sphere with a center charge has been studied in [1]. Using the rotational symmetry, the 3D nonlinear PBE can be reduced to a one-dimensional (1D) boundary value problem. By taking the length of the truncated interval to be 100 times of the sphere radius, the Dirichlet zero condition can be safely assumed. Based on an eighth order finite difference discretization, a high-precision nonlinear energy can be calculated as a reference energy, whose numerical error is shown to be around 10^{-12}. Moreover, a benchmark study has been carried out in [1] by using the regularized Matched Interface and Boundary (rMIB) package [18], which is a well-established second-order accurate PBE solver with advanced 3D treatments to address four out of five difficulties mentioned above, i.e., singularity [17,18,24], molecular surface [40,43], interface jumps [43,47], and nonlinearity [9]. In the linearized case, the Kirkwood sphere problem admits an analytical solution. By using this analytical solution as the Dirichlet boundary condition, the rMIB package achieved a second order of convergence in calculating both potential and energy [1]. Nevertheless, by using the same Dirichlet boundary condition for the nonlinear PBE, the rMIB result fails to converge to the reference energy [1].

To overcome the limitations of the Dirichlet boundary conditions, several other types of boundary conditions have been proposed for the nonlinear PBE [5,30,35]. In [30], a self-consistent boundary (SCB) condition is introduced by multiplying the linearized PBE in the solvent by its fundamental solution under a unit charge and then integrating over the domain Ω. This yields an expression of the potential u in terms of surface integrals of the potential u, the Green's function and their gradients, over the boundary $\partial\Omega$. The SCB condition is implemented in an iterative procedure, in which the surface integrals are calculated based on the previous iterative step to produce Dirichlet boundary values for the present iteration. The SCB condition is actually a global boundary condition in the sense that one boundary value is related to all boundary values on $\partial\Omega$ and the iterative calculation of boundary integrals is quite expensive.

In [35], a novel asymptotic boundary analysis has been conducted based on analytical approximations of the nonlinear PBE. In particular, by modeling the molecular system as a spherically symmetric one and approximating the hyperbolic Sine term by the first two terms in the Taylor series expansion, the 3D PBE is reduced to a 1D nonlinear ordinary differential equation (ODE), whose asymptotic solution is shown to have the same decaying function as in the linear case. Moreover, the nonlinear constant behind the decaying function is proposed to be calculated as the sum of the linear constant and two perturbation terms. This asymptotic boundary condition has been tested for a few molecular systems in [35], but a widespread application to general problems without spherical symmetry remains unexplored.

In [5], Boschitsch and Fenley also found that the nonlinear PBE in a spherically symmetric setting admits the same asymptotic function as in the linear case. The constant behind the decaying function is proposed to be calculated by a line integral of the nonlinear term in the radial direction over the solvent domain. This new outer boundary formulation allows the authors to formulate energy

corrections to account for contributions from outside the spherical domain [5]. Moreover, this boundary treatment can be extended to non-symmetric cases on cubic domains, in which the asymptotic constant is calculated based on the potential in the previous iterative step and through a volume integral of the nonlinear term over some solvent region. The extended boundary approach has been successfully applied to a fast and robust PBE solver based on adaptive Cartesian grids for electrostatic analysis of a large set of proteins [6]. This asymptotic boundary approach is also a global boundary condition, in which boundary values on six sides of the cubic domain depend on all potential values in the solvent region, and the iterative calculation of volume integrals could be expensive.

The goal of this paper is to develop a simple local boundary condition that is valid for both the linear and nonlinear PBE. Based on the same asymptotic solution considered in [5,35] for the asymptotically symmetric nonlinear PBE, a modified Robin boundary condition involving a radial derivative is introduced. For general protein systems, the radial direction can be defined based on the geometrical center of the protein. Physically, as pointed out in [5], the reason why this asymptotic boundary formulation works for non-symmetric cases [6] is that at sufficiently large distance from the macromolecule, the monopole representation of all partial charges dominates higher moments, such as dipoles and quadrupoles [23,38]. Mathematically, unlike the existing asymptotic boundary conditions [5,30,35], the proposed Robin condition is a local boundary condition, i.e., one boundary value only relates to its derivatives at the same point.

A local boundary condition allows a much simpler implementation and faster computation than a global condition. The proposed Robin boundary condition can be applied to any finite difference and finite element PBE solvers. Without resorting to an iterative procedure, the modified Robin condition enforcement can be directly built in the spatial discretization matrix and only involves a few nearby grid nodes or sparse coefficients. In this work, a ray-casting matched interface and boundary (MIB) technique will be developed to implement the proposed Robin condition as a second order accurate boundary scheme in a Cartesian grid finite difference setting. To demonstrate its performance, this boundary scheme will be embedded in the rMIB package [18] so that the enhanced rMIB PBE solver can handle all five difficulties mentioned above.

The rest of the paper is organized as follows: Section 2 provides an overview of the PB model and the commonly used boundary conditions for electrostatic analysis of proteins. The key formulation of the rMIB PBE solver [18] will also be discussed. The spherical symmetric PBE will be concerned in Section 3 to derive the proposed Robin boundary condition. High order 1D finite difference methods will be employed to illustrate the accuracy of the new boundary condition in treating the Kirkwood sphere in both linear and nonlinear cases. The generalization of the modified Robin boundary condition to non-symmetric cubic domains will be presented in Section 4. A ray-casting MIB scheme will be constructed to discretize the modified Robin condition in the rMIB package. Various numerical experiments will be conducted in Section 5 to examine the accuracy, robustness, and efficiency of the proposed boundary scheme, and comparison with Dirichlet boundary conditions will be studied too. Finally, the paper ends with a conclusion and future plan in Section 6.

2. PBE model and rMIB PB solver

In this section, we will first describe the Poisson-Boltzmann (PB) equation, followed by a discussion of the commonly used Dirichlet boundary conditions for the PB equation. This section also provides an overview of the 3D regularized Matched Interface and Boundary (rMIB) PB solver, which is the main testbed for the new development.

2.1. The Poisson-Boltzmann equation (PBE)

The Poisson-Boltzmann equation (PBE) as illustrated in Fig. 1 is the governing equation of electrostatics of a solute macromolecular immersed in an aqueous solvent environment. A computational domain $\Omega \subset \mathbb{R}^3$ is usually assumed in grid-based numerical computations, which is divided into two subdomains, Ω^- and Ω^+, by the molecular surface Γ. The subdomain Ω^- represents the molecular region while the subdomain Ω^+ is the solvent region, i.e., $\Omega = \Omega^- \cup \Omega^+$. The outer boundary of Ω is denoted by $\partial\Omega$. The partial charges on the solute molecule are assigned to each atom by a force field while the mobile ions in Ω^+ are charges described by the Boltzmann distribution.

The electrostatic interaction of the solute-solvent system is modeled by the nonlinear PBE

$$\begin{cases} -\nabla \cdot (\epsilon(\mathbf{r})\nabla u(\mathbf{r})) + \bar{\kappa}^2(\mathbf{r}) \sinh(u(\mathbf{r})) = \rho(\mathbf{r}), & \mathbf{r} \in \Omega \\ [u]_\Gamma = 0, & \mathbf{r} \in \Gamma \\ [\epsilon \frac{\partial u}{\partial n}]_\Gamma = 0, & \mathbf{r} \in \Gamma, \end{cases} \tag{1}$$

subject to an appropriate boundary condition at $\partial\Omega$. Here $u(\mathbf{r})$ is the dimensionless electrostatic potential [46], vanishing at infinity, namely

$$u(\mathbf{r}) = 0, \quad \text{as } |\mathbf{r}| \to \infty. \tag{2}$$

The singular source term $\rho(\mathbf{r})$ is defined as

$$\rho(\mathbf{r}) = 4\pi \frac{e_c^2}{k_B T} \sum_{i=1}^{N_m} q_i \delta(\mathbf{r} - \mathbf{r}_i),$$

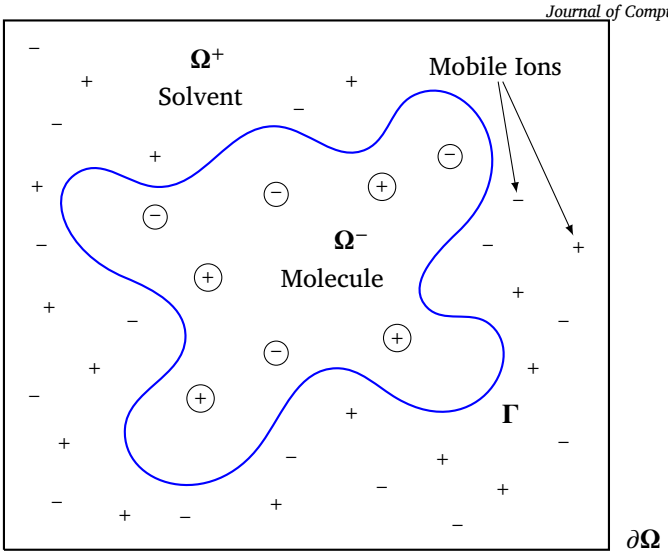

Fig. 1. A 2D illustration of the 3D PB domain.

where N_m is the number of atoms in the solute molecule with each atom carrying a dimensionless partial charge q_i, located at $\mathbf{r}_i$. Here, δ is the Dirac delta function, e_c is the fundamental charge, k_B is the Boltzmann constant and T is the absolute temperature.

In Eq. (1), the dielectric constant, $\epsilon(\mathbf{r})$, is a dimensionless piecewise constant which is represented as ϵ^- in Ω^- and ϵ^+ in Ω^+. The modified Debye-Hückel parameter, $\bar{\kappa}(\mathbf{r})$, is a piecewise constant measuring the concentration of ions in the solution. It is defined as $\bar{\kappa} = 0$ in Ω^- and as $\bar{\kappa}^2 = 8.430325455\ \text{Å}^{-2} I$, for $T = 300K$, in Ω^+. The dimensionless constant I is the ionic strength of the solution and the unit of $\bar{\kappa}^2$ is Å^{-2}, where Å is the angstrom.

The nonlinear PBE Eq. (1) is subject to the jump conditions $[u]_\Gamma$ and $[\epsilon \frac{\partial u}{\partial n}]_\Gamma$ across the interface, Γ. Here, $\mathbf{n} = (n_x, n_y, n_z)$ is the outer normal direction of the interface and $u_n = \frac{\partial u}{\partial n}$ is the directional derivative. The difference between the functional values across the interface Γ, is denoted by $[f]_\Gamma = f^+ - f^-$. Details of the units of the PBE are described in [20].

When the dimensionless potential u is weak, the nonlinear term $\sinh(u)$ in Eq. (1) can be linearized as u, giving rise to the linearized PBE

$$-\nabla \cdot (\epsilon(\mathbf{r})\nabla u(\mathbf{r})) + \bar{\kappa}^2(\mathbf{r})u(\mathbf{r}) = \rho(\mathbf{r}), \quad \mathbf{r} \in \Omega \tag{3}$$

subject to the same interface jump conditions on Γ as in Eq. (1) and an appropriate boundary condition on ∂Ω.

2.2. Commonly used boundary conditions for PBE

The PBE over an infinite domain satisfies the asymptotic condition Eq. (2). However, for grid-based methods, a finite computational domain Ω has to be used, and a boundary condition on ∂Ω is required. To define Ω in a finite difference computation, a tight cuboid box that exactly encloses the solute region or molecular surface is usually first determined. Then an edge value is used to enlarge this box in both positive and negative directions along x, y, and z coordinates, which defines the computational domain Ω [18]. In other words, the edge value measures the distance between the molecular surface and the boundary along the Cartesian directions. In protein simulations, since the dimension of the macromolecular is already very large, a small edge value is preferred to save the computational cost. This demands an accurate and robust boundary condition for the PB model.

When the domain size is very large, a Dirichlet zero boundary condition could be assumed

$$u(\mathbf{r}) = 0, \quad \mathbf{r} \in \partial\Omega. \tag{4}$$

For example, in studying the Kirkwood sphere with a central charge [1], a very large domain size can be used, because the 3D PBE has been reduced to a 1D problem using the spherical symmetry. By taking the domain length as 100 times of the sphere radius, the energies computed in [1] for both linear and nonlinear PBE cases could reach a precision on the order of 10^{-12}. However, the energy error grows rapidly as the domain length becomes smaller for the Dirichlet zero condition.

The most commonly used boundary condition for the PB model is the Debye-Hückel condition [20]

$$u(\mathbf{r}) = \frac{e_c^2}{k_B T} \sum_{i=1}^{N_m} \frac{q_i e^{-\lambda|\mathbf{r}-\mathbf{r}_i|}}{\epsilon^+ |\mathbf{r}-\mathbf{r}_i|}, \quad \mathbf{r} \in \partial\Omega, \tag{5}$$

where $\lambda = \sqrt{\frac{\bar{\kappa}^2}{\epsilon^+}}$. This condition is obtained from an analytical solution of the linearized PBE Eq. (3) under the fully penetrating assumption that the solvent medium occupies the entire $\mathbb{R}^3$ space and each atom is treated as a point charge q_i at $\mathbf{r}_i$. This Dirichlet boundary condition has been widely used in many PBE solvers, such as [9,10,17–19,26,36], and will be further studied in this work.

A multiple Debye-Hückel (MDH) Dirichlet boundary condition used in the APBS package [3] can be regarded as a modified form of Eq. (5)

$$u(\mathbf{r}) = \frac{e_c^2}{k_B T} \sum_{i=1}^{N_m} \frac{q_i e^{\lambda(a_i - |\mathbf{r}-\mathbf{r}_i|)}}{\epsilon^+(\lambda a_i + 1)|\mathbf{r}-\mathbf{r}_i|}, \quad \mathbf{r} \in \partial\Omega, \tag{6}$$

where a_i stands for the radius of i^{th} atom. In fact, when each atom shrinks to a point charge, i.e., $a_i = 0$, Eq. (6) becomes Eq. (5). When only one atom is concerned, Eq. (6) yields

$$u(\mathbf{r}) = \frac{e_c^2}{k_B T} \frac{q e^{\lambda(a - |\mathbf{r}-\mathbf{r}_c|)}}{\epsilon^+(\lambda a + 1)|\mathbf{r}-\mathbf{r}_c|}, \quad \text{for } |\mathbf{r}-\mathbf{r}_c| \geq a, \tag{7}$$

which is the analytical solution of the linearized PBE for the Kirkwood sphere [1] with the radius being a and center located at $\mathbf{r}_c$. Thus, the MDH Dirichlet boundary condition Eq. (6) is essentially an approximate solution to the linearized PBE based on the superposition of N_m Kirkwood spheres, while neglecting their mutual interactions.

It is known in the literature [1] that the application of Dirichlet boundary conditions derived from the linearized PBE to the nonlinear PBE can be problematic. This work aims to address the limitations of the existing Dirichlet conditions by proposing a new boundary condition that is accurate and efficient for 3D PBE simulations.

2.3. 3D regularized Matched Interface and Boundary (rMIB) PB solver

Before we discuss the derivation of the new boundary condition and its implementation, we first review the three-dimensional (3D) regularized Matched Interface and Boundary (rMIB) PB solver [18], which is the primary 3D PB solver used in this work. As mentioned previously, the numerical solution of the PBE in 3D suffers five particular challenges. The rMIB package is a second order accurate finite difference solver that is equipped with advanced numerical treatments to address four difficulties out of the five, i.e., singularity, dielectric interface, molecular surface, and nonlinearity. The following overview will focus on these four items.

(1) Singularity. It is well known that the electrostatic potential u of the PBE will blow up at each atom center, i.e., $u \to \infty$ as $\mathbf{r} \to \mathbf{r}_i$, due to singularities in the source term $\rho(\mathbf{r})$. To treat the singularities, a two-component regularization method is proposed in [18], which decomposes the electrostatic potential in Ω^- into two components, namely, the reaction field component u_{RF} and the Coulomb component u_C, with $u^- = u_C + u_{RF}$. The Coulomb component satisfies the Poisson equation with the same singular source $\rho(\mathbf{r})$,

$$\begin{cases} -\epsilon^- \Delta u_C(\mathbf{r}) = \rho(\mathbf{r}), & \mathbf{r} \in \mathbb{R}^3 \\ u_C(\mathbf{r}) = 0, & \text{as } |\mathbf{r}| \to \infty, \end{cases} \tag{8}$$

where u_C is analytically given as the Green's function Eq. (9)

$$G(\mathbf{r}) = \frac{e_c^2}{k_B T} \sum_{i=1}^{N_m} \frac{q_i}{\epsilon^- |\mathbf{r}-\mathbf{r}_i|}. \tag{9}$$

By substituting Eq. (8) into Eq. (1), a regularized PBE can be derived [18]

$$\begin{cases} -\nabla \cdot (\epsilon \nabla \tilde{u}) + \bar{\kappa}^2 \sinh(\tilde{u}) = 0, & \text{in } \Omega \\ [\tilde{u}]_\Gamma = G, & \text{on } \Gamma \\ [\epsilon \frac{\partial \tilde{u}}{\partial n}]_\Gamma = -\epsilon^- \frac{\partial G}{\partial n}, & \text{on } \Gamma, \end{cases} \tag{10}$$

where the regularized potential $\tilde{u}$ is defined as

$$\tilde{u} = \begin{cases} u_{RF}, & \text{in } \Omega^- \\ u, & \text{in } \Omega^+. \end{cases} \tag{11}$$

In other words, the potential u is not split in the solvent domain Ω^+. After solving $\tilde{u}$ from Eq. (10), the original potential in the solute region is recovered by adding the Green's function to the reaction field potential, that is, $u = \tilde{u} + G = u_{RF} + G$, while the potential in the solvent region is recovered as $u = \tilde{u}$. Recently, a comparison of the two-component regularization of the rMIB algorithm [18] with three other popular PBE regularization methods involving two or three components has been conducted [24], and it is found that the rMIB regularization is both the most accurate and the most efficient approach.

In this work, the numerical results will be benchmarked by computing the electrostatic free energy. In terms of the dimensionless potential u, the calculation of the electrostatic free energy has been discussed in details in [46] without any unit conversion. In the present work, without considering the electrostatic stress and excess osmotic pressure of the mobile ions, the electrostatic free energy for both linear and nonlinear PB models will be computed as

$$E = \frac{1}{2} k_B T \sum_{i=1}^{N_m} q_i u_{RF}(\mathbf{r}_i). \tag{12}$$

As discussed in the two-component regularization method [18], the electrostatic potential in the vacuum phase is simply given by the Green's function Eq. (9). Thus, the difference between the potentials in water and vacuum phases is actually the reaction field potential u_{RF}. Moreover, the surface integrals can usually be dropped in energy computation of protein systems [46]. Then, the energy expression can be given as Eq. (12).

(2) Dielectric interface. Across the dielectric interface Γ with discontinuous coefficients, the regularized potential $\tilde{u}$ is discontinuous according to the jump conditions given in Eq. (10). Without proper treatments, the standard finite difference (FD) method will lose its accuracy at the interface. In fact, the regularization PBE Eq. (10) and the original PBE Eq. (1) are typical examples of elliptic interface problems [12,47] – a well-known challenge in scientific computing. By using a Cartesian grid finite difference discretization, the key issue in solving elliptic interface problems is on how to restore the accuracy near the interface.

To overcome this challenge and to ensure accurate electrostatic calculations, the rMIB PB solver uses the Matched Interface and Boundary (MIB) scheme [47], a robust high order numerical scheme for interface equations with discontinuous coefficients. The main idea of the MIB scheme is that when the finite difference stencil refers to a point from the other side of the interface, a fictitious value instead of the original function value will be used. The fictitious values can be regarded as a smooth extension of potential solutions from one side of the interface to the other side. Numerically, they are generated rigorously by enforcing the jump conditions. A Cartesian MIB scheme is employed in the rMIB package, i.e., the jump conditions in the normal direction will be decomposed into x, y and z directions, and the Cartesian jump conditions will be discretized by finite difference involving fictitious values and original potentials. Then, the fictitious points can be solved as a linear combination of the grid values and jump data, allowing them to be substituted into the Laplacian FD discretization. The MIB scheme is able to treat 3D complicated interfaces including sharp edge corners [43,44], and has been successfully applied as a second order accurate PB solver for protein simulations [9,17,18,43].

(3) Molecular surface. In the PBE literature, the solute-solvent boundary Γ is usually taken as the solvent excluded surface (SES) [25,34], which is defined with a solvent molecule probe that rolls around the Van der Waals spheres representing all atoms. The MSMS program [37] is a popular software for generating the SES efficiently based on a reduced surface, which provides a Lagrangian representation of the SES by means of a triangulated surface mesh. In order to generate the necessary interface and jump data for the MIB treatments, a Lagrangian-to-Eulerian conversion is required to convert the MSMS triangulation into Cartesian grids. This is numerically challenging because the SES molecular surface is known to have geometrical singularities. Fortunately, advanced Lagrangian-to-Eulerian development has been developed in [9,43] so that the rMIB package works well for the MSMS surface [18]. Recently, an Eulerian Solvent Excluded Surface (ESES) algorithm [27] has been constructed to directly calculate the analytical SES patches based on Cartesian grids, which provides an easy generation of interface data for the MIB scheme. More recently, the rMIB package has been extended to include the ESES surface [40]. In the present study, the new boundary condition will be tested with the rMIB-MSMS version [18], while it should work equally well for the rMIB-ESES version [40].

(4) Nonlinearity. The rMIB PB solver [18] employs the inexact-Newton method [9,21] for treating the PBE nonlinearity, and the sparse linear systems inside each Newton iteration are solved by the Bi-conjugate gradient (BCG) algorithm. Here, the inexactness means that a large tolerance value, e.g. 10^{-2}, can be used in the BCG solution, because the overall accuracy of the nonlinear solution is mainly controlled by the outside Newton's iteration. Recently, a comparison of the inexact-Newton method and a relaxation scheme based on the same MIB spatial discretization has been conducted in [33]. By calculating the nonlinear term from the previous iteration in the relaxation approach, the discretization of the Laplacian operator can take advantage of the fast Fourier-transform (FFT) fast Poisson solver and the augmented MIB (AMIB) algorithm [12] for potential acceleration. Consequently, the FFT-AMIB algorithm could be faster than the inexact-Newton method in Kirkwood sphere tests. However, for real proteins, an extended domain with extra unknowns is required in the FFT-AMIB procedure, because the mesh size in each Cartesian direction has to be increased to be powers of 2. Therefore, the inexact-Newton method has been found to be more efficient than the FFT relaxation method in protein studies [33].

3. Kirkwood sphere and modified Robin boundary condition

In this section, we will propose a modified Robin boundary condition for the nonlinear PBE in a spherically symmetric setting. To this end, a Kirkwood sphere with a centered charge q at the origin $(0,0,0)$ and radius being a will be studied for both linear and nonlinear cases [1]. Numerical simulations for the 1D PB model will be carried out to validate the proposed Robin boundary condition.

3.1. Modified Robin boundary condition

Using the spherical symmetry, the 3D nonlinear PBE Eq. (1) for the Kirkwood sphere can be reduced to a 1D ordinary differential equation (ODE) in the radial direction $r = |\mathbf{r}|$. In particular, the potential $u(r)$ in the solvent domain Ω^+ outside the radius $r = a$ satisfies the following boundary value problem (BVP) [1],

$$\begin{cases} u'' + \frac{2}{r}u' - \lambda^2 \sinh(u) = 0, & r \in [a, \infty) \\ u'(r) = -\frac{\epsilon_c^2}{k_B T} \frac{q}{\epsilon^+ r^2}, & r = a \\ u = 0, & r \to \infty, \end{cases} \tag{13}$$

where $u'(r) = \frac{du}{dr}$ and $\lambda = \sqrt{\frac{\bar{\kappa}^2}{\epsilon^+}}$. The Neumann boundary condition at the left boundary is derived based on the analytical solution in the solute domain Ω^- and two jump conditions at the interface $r = a$ [1]. Computationally, the infinity domain $[a, \infty)$ has to be truncated to a finite domain $[a, b]$. When a large enough b is chosen, a Dirichlet zero boundary condition (DBC0), Eq. (4), may be assumed at $r = b$ with a negligibly small truncation error [1].

Similarly, the 3D linearized PBE for the Kirkwood sphere gives rise to a 1D BVP [1]

$$\begin{cases} u'' + \frac{2}{r}u' - \lambda^2 u = 0, & r \in [a, \infty) \\ u'(r) = -\frac{e_c^2}{k_B T}\frac{q}{\epsilon^+ r^2}, & r = a \\ u = 0, & r \to \infty, \end{cases} \tag{14}$$

which admits an analytical solution

$$u(r) = \frac{e_c^2}{k_B T}\frac{q e^{\lambda(a-r)}}{\epsilon^+(\lambda a + 1)r}, \quad \text{for } r \geq a. \tag{15}$$

For a general Kirkwood sphere with radius a and center $\mathbf{r}_c$, the analytical solution in 3D is given by Eq. (7) with $r = |\mathbf{r} - \mathbf{r}_c|$.

Consider a modest b value for the nonlinear 1D PBE Eq. (13), for which the Dirichlet zero boundary condition, Eq. (4), is not applicable. Without the loss of the generality, one can assume $u(r) \ll 1$ near the right boundary $r = b$. Consequently, $\sinh(u)$ in Eq. (13) can be approximated by the first term in the Taylor series expansion, i.e., $\sinh(u) \approx u$. Therefore, the asymptotic solution of the nonlinear PBE near $r = b$ can be approximated by the Kirkwood solution $u(r)$ given in Eq. (15). This suggests that the following analytical boundary condition (ABC) could be used as an approximate boundary condition for the nonlinear PBE Eq. (13)

$$u(r) = \frac{e_c^2}{k_B T}\frac{q e^{\lambda(a-r)}}{\epsilon^+(\lambda a + 1)r} := C_L \frac{e^{-\lambda r}}{r}, \quad \text{at } r = b, \tag{16}$$

where the linear constant $C_L = \frac{e_c^2}{k_B T}\frac{q e^{\lambda a}}{\epsilon^+(\lambda a+1)}$. Moreover, as pointed out in both Ref. [35] and Ref. [5], it could be assumed that the potential of the nonlinear PBE has the same asymptotic decaying rate as in the linearized case near $r = b$, which yields the following asymptotic boundary condition

$$u(r) = C_{NL}\frac{e^{-\lambda r}}{r}, \quad \text{at } r = b. \tag{17}$$

Such a Dirichlet condition could provide a better approximation than Eq. (16), if the nonlinear constant C_{NL} can be accurately estimated. In [35], the nonlinear constant is proposed to be calculated as the sum of the linear constant C_L and two perturbation terms, while in [5], C_{NL} is calculated by a volume integral of the nonlinear term in the radial direction over the solvent domain. Numerically, the volume integrals are computed by using potential values in the previous iterative step [5].

In the present study, a novel Robin boundary condition is proposed, in which the difficulty in estimating C_{NL} in Eq. (17) is simply bypassed. In particular, by taking derivative of Eq. (17), we have

$$\frac{du}{dr} = -C_{NL}\frac{e^{-\lambda r}}{r}\left(\lambda + \frac{1}{r}\right) = -u(r)\left(\lambda + \frac{1}{r}\right), \quad \text{for } r \text{ near } b. \tag{18}$$

This gives rise to a modified Robin boundary condition,

$$\frac{du}{dr} + \left(\frac{1}{r} + \lambda\right)u(r) = 0, \quad \text{at } r = b, \tag{19}$$

which is valid for both LPB and NPB models. The proposed Robin boundary condition (RBC) Eq. (19) does not involve any unknown parameters. Moreover, it is a local boundary condition, i.e., one boundary value only relates to its derivatives at the same point.

3.2. Asymptotic validation of the RBC

The derivation of the RBC, Eq. (19), is based on an assumption that at the right boundary $r = b$, we have $u \ll 1$. This may raise a concern that b has to be quite large. In this subsection, we use 1D numerical solutions for both LPB and NPB cases to show that the proposed RBC is actually very robust so that b does not need to be much larger than a, i.e., we just need $b > a$, without requiring $b \gg a$. To this end, we will first verify that the potentials for both linear and nonlinear cases have the same asymptotic decaying form

$$u(r) = C\frac{e^{-\lambda r}}{r}, \quad \text{for } r > a, \tag{20}$$

while the constant C could be slightly different for linear and nonlinear cases. Note that as long as Eq. (20) is valid at a point $r > a$, the RBC Eq. (19) is valid at the same point.

We consider the numerical solution of the 1D BVPs for nonlinear PBE Eq. (13) and linearized PBE Eq. (14) over a finite domain $[a, B]$ with a DBC0 condition $u(B) = 0$. An eighth order accurate MIB scheme [1] is employed to discretize two BVPs. The parameters of the Kirkwood sphere are chosen as $a = 2$ Å, $q = 1$, $\epsilon^- = 1$, $\epsilon^+ = 80$, and $I = 0.15$. By using a sufficient large B and a small enough mesh spacing h (both in a unit of Å), the MIB scheme can produce accurate approximations to potential and electrostatic energy with errors on the order of 10^{-12} [1]. By fixing the dimension as $N = 6401$, we test several B values. For each tested domain $[a, B]$,

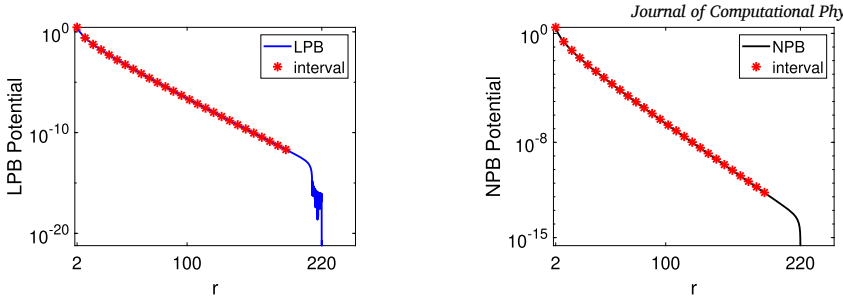

(a) LPB Electrostatic Potential (b) NPB Electrostatic Potential

Fig. 2. Plot of 1D LPB and NPB potentials of the Kirkwood sphere in the log scale. The computational domain is $[2, 220]$ with a DBC0 boundary condition at $B = 220$. To avoid the boundary pollution, a suitable data interval is chosen in each case, which is marked with red stars.

Table 1
Asymptotic analysis for 1D LPB and NPB potentials of the Kirkwood sphere with $N = 6401$ and different B values.

	LPB			NPB		
B (Å)	$\ln K$	α	β	$\ln K$	α	β
160	1.708481	0.129379	-0.875493	1.671415	0.129269	-0.880617
180	1.796767	0.127825	-0.921089	1.757976	0.127745	-0.925331
200	1.947021	0.125959	-0.990668	1.948454	0.125944	-0.991310
220	1.966224	0.125742	-0.999330	1.924385	0.125700	-1.002151

we select a range of potential solution values $u_i := u(r_i)$ for $i = 1, 2, \ldots, n$, and conduct a least squares (LS) data fitting to detect the asymptotic decaying pattern, which is assumed to be

$$u(r) = K e^{-\alpha r} r^{\beta}. \tag{21}$$

Asymptotically, it is expected that $\alpha \to \lambda = 0.12572533646057585$ Å^{-1}, $\beta \to -1$ and $K \to C$ Å, when $B \to \infty$ and $h \to 0$. Note that the potential u is dimensionless in the present study [46]. Taking the natural logarithm of Eq. (21), we arrive at a multilinear least squares problem

$$\begin{bmatrix} 1 & -r & \ln r \end{bmatrix} \begin{bmatrix} \ln K \\ \alpha \\ \beta \end{bmatrix} = \begin{bmatrix} \ln u \end{bmatrix}. \tag{22}$$

For a data set with (r_i, u_i) for $i = 1, 2, \ldots n$, Eq. (22) can be rewritten into a matrix form $Ax = f$, where $A \in \mathbb{R}^{n\times 3}$ consists of three columns with ones, $-r_i$ and $\ln r_i$, $x = [\ln K, \alpha, \beta]^T$, and $f \in \mathbb{R}^n$ with entries $\ln u_i$.

Note that the data range for (r_i, u_i) starts from $i = 1$ or $r_1 = a$. For each tested domain $[a, B]$, a suitable n value has to be chosen. As shown in Fig. 2, near the boundary $r = B$, the potential u deviates from the asymptotic decaying pattern, because of the boundary condition $u(B) = 0$. Thus, n has to be carefully chosen so that the boundary pollution could be avoided.

By considering four large B values, the LS fitted asymptotic parameters are reported in Table 1. It is obvious that as B increases, we have $\alpha \to \lambda$ and $\beta \to -1$ for both linear and nonlinear cases. A few remarks are in order. First, the convergence patterns of α towards λ for both linear and nonlinear cases are quite similar. This demonstrates that the NPB potential has the same asymptotic decaying as the linear case. Second, it should be emphasized that the data range in the present analysis starts from $r_1 = a$. In other words, the asymptotic solution Eq. (20) holds for any $r > a$. Computationally, this means that proposed RBC Eq. (19) will be valid for any b value with $b > a$, without requiring $b \gg a$. Third, the constant K approaches slightly different limits for linear and nonlinear cases in Table 1. This indicates that C_{NL} is indeed different from C_L in Eq. (17) and Eq. (16), respectively. This justifies the efforts in [5,35] for estimating C_{NL} numerically. Nevertheless, the need to calculate the asymptotic constant is simply eliminated in the proposed RBC.

3.3. Numerical validation of the RBC in 1D

In this subsection, we examine the performance of the RBC Eq. (19) by solving the following 1D BVP of the nonlinear PBE

$$\begin{cases} u'' + \frac{2}{r}u' - \lambda^2 \sinh(u) = 0, & r \in [a, b] \\ u'(r) = -\frac{e_c^2}{k_B T} \frac{q}{\epsilon^+ r^2}, & r = a \\ u'(r) + \left(\frac{1}{r} + \lambda\right) u(r) = 0, & r = b. \end{cases} \tag{23}$$

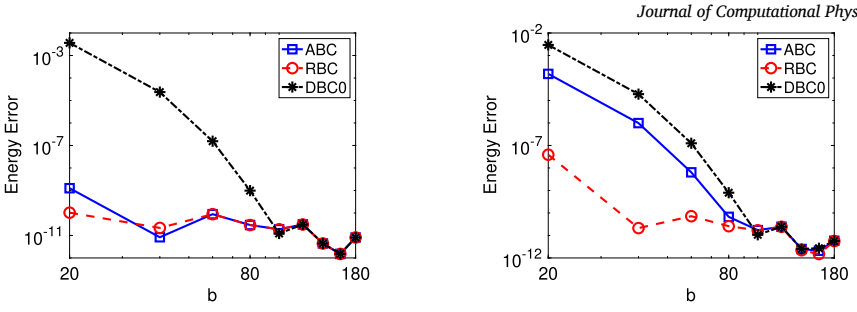

Fig. 3. Energy errors of the Kirkwood sphere for three boundary conditions with a fixed mesh size $N = 6401$ and different domain size b. (a) LPB; (b) NPB.

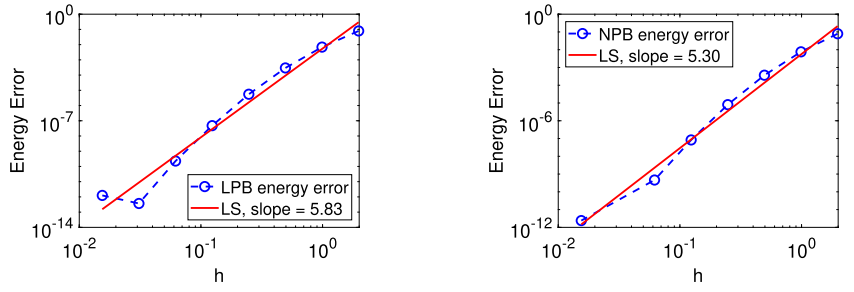

Fig. 4. Energy errors of the Kirkwood sphere for the RBC with a fixed domain size $b = 200$ Å and different spacing h. (a) LPB; (b) NPB.

Similarly, the corresponding BVP of the linearized PBE, obtained by replacing $\sinh(u)$ with u in Eq. (23), will also be studied. For comparison, we will also solve other four BVPs for linearized and nonlinear PBEs. Two of them use the DBC0 condition, Eq. (4), at $r = b$, while the other two employs the ABC condition, Eq. (16), at $r = b$. Note that the ABC condition is exact for the linear Kirkwood sphere, but is just an approximate condition for the nonlinear case. The eighth order MIB scheme [1] will be employed to discretize all BVPs.

In the present study, the parameters of the Kirkwood sphere are chosen as $a = 2$ Å, $q = 1$, $\epsilon^- = 1$, $\epsilon^+ = 80$, and $I = 0.15$. For the linearized case, the electrostatic free energy has an analytical value for the Kirkwood sphere, i.e., $E = -82.188683337726175\, kcal/mol$. For the nonlinear Kirkwood sphere, a benchmark procedure has been developed in [1], and the reference energy can be calculated as $E = -82.212210265417710\, kcal/mol$, whose precision is about 10^{-12}.

We first test the energy error by considering different domain size b with a fixed dimension $N = 6401$. It can be seen from Fig. 3a that in the LPB case, the RBC condition produces negligible energy errors for all b values, which are as good as the ABC condition. The DBC0 invokes large errors when b is small, and a large b value such as $b = 100$ has to be used for producing similar errors as other conditions. For the NPB case in Fig. 3b, the RBC condition obviously dominates the other two, and delivers the best accuracy for all b values. The ABC condition becomes an approximate one, so that it is just slightly better than the DBC0.

We next examine the convergence of the RBC for successive mesh refinements. By using a fixed domain size $b = 200$ Å, we compute energy errors at different h values for both linear and nonlinear cases. It can be seen from Fig. 4 that such errors become vanishing as h goes to zero. In the LPB case, the precision limit of the iterative solver has been reached so that the error stops decreasing in the end. A least squares (LS) fitting has been conducted in the log scale for detecting the numerical convergence orders, which are found to be 5.83 and 5.30, respectively, for linear and nonlinear Kirkwood spheres. This indicates that the MIB spatial discretization is of high order convergence.

It is known in [5] that the usual Dirichlet boundary condition could produce unphysical solutions for a highly charged biomolecule. For the present Kirkwood sphere problem, we also consider a highly charged system with the centered charge $q = 50$ and radius $a = 10$ Å, while other parameters are kept the same. Here, we only show the results for the nonlinear PB model, whose reference energy $E = -41413.479350115194\, kcal/mol$, is generated by using the 1D solver developed in [1].

For the highly charged Kirkwood sphere, we first examine the energy errors against the domain size b with a fixed dimension $N = 4336$. It can be seen from Fig. 5a that the energy errors of the ABC and DBC0 conditions are large for small b values. The RBC condition is obviously the best among the three, and produces accurate energies regardless of the value of b.

To see why the ABC condition fails in the nonlinear case for the highly charged Kirkwood sphere, the plot of electrostatic potential u against $r \in [10, 20]$ is depicted in Fig. 5b. Here, the domain size is chosen as $b = 20$ Å with $N = 4336$. For the DBC0 condition, the potential u equals zero at the right boundary, which in some sense pulls the potential curve down so that the DBC0 potential disagrees with the other two throughout. The ABC on the other hand produces some unphysical pattern, i.e., the potential is a non-decaying function that attains a minimum within the finite interval. Only the RBC delivers a reasonable asymptotic pattern – the potential is decaying while it does not equal zero at a finite r value.

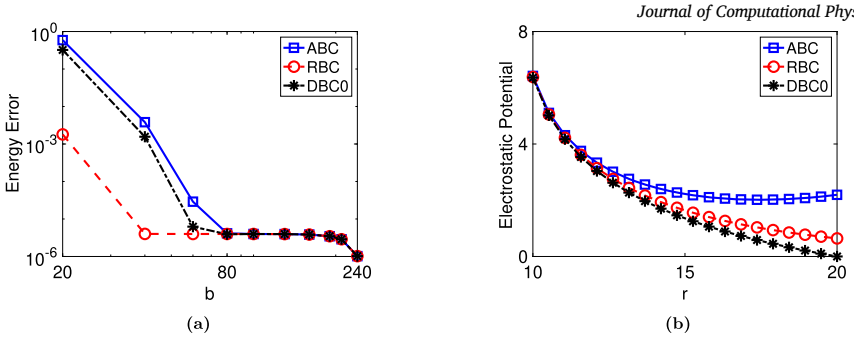

Fig. 5. Numerical results of three boundary conditions for a highly charged Kirkwood sphere ($a = 10$ Å, $q = 50$) by using a fixed mesh size $N = 4336$. (a) Energy errors with different domain sizes b. (b) Electrostatic potential u with a fixed domain size $b = 20$ Å and the plot is over the interval $r \in [10, 20]$.

The 1D numerical results presented in this section demonstrate that the proposed Robin boundary condition Eq. (19) outperforms the analytical Dirichlet condition and Dirichlet zero condition for both linearized and nonlinear PB models, irrespective of domain sizes, radii, or charge values. Since the 1D modeling is limited to the PBE with spherical symmetry, we will investigate the performance of the proposed RBC for 3D protein simulations over non-symmetric Cartesian domains in the next section.

4. Robin boundary condition for proteins and its implementation in 3D

The proposed Robin boundary condition (RBC) Eq. (19) can be generalized for truncating the nonlinear PB model over non-symmetric cubic domains. Theoretical and asymptotic analysis will be conducted in this section to justify the RBC for biomolecular simulations. A second order finite difference scheme will be proposed for implementing the RBC on Cartesian grids in 3D.

4.1. The RBC for 3D non-symmetric systems

Consider a biomolecule with N_m atoms. For each atom, its radius is a_i with the unit Å, and a partial charge q_i is located at its center $\mathbf{r}_i = (x_i, y_i, z_i)$. The electrostatic potential is governed by the nonlinear PBE Eq. (1) over the infinity domain, while the solute-solvent interface Γ is assumed to be the solvent excluded surface (SES) [25,34].

The proposed RBC Eq. (19) can be reformulated to provide a new boundary condition for the nonlinear PBE Eq. (1) so that a truncated computational domain Ω can be used. The theoretical justification of the RBC for non-symmetric cubic domains consists of two physical considerations.

First, away from the biomolecular, it is assumed that $\sinh(u)$ could be approximated by u so that the asymptotic solution near the boundary $\partial\Omega$ can be modeled by the linearized PBE. It is noted that the edge value defining the domain Ω does not need to be large enough such that $u \ll 1$. The RBC is very robust so that the usual edge value used in the rMIB package [18] will be sufficient.

Second, it is assumed that near $\partial\Omega$, the monopole term dominates the asymptotic solution – the same argument has been considered in [5,35] for deriving boundary conditions for the nonlinear PBE. Physically, away from the biomolecule, the electrostatic potential induced by the arbitrary charge distribution contained in the biomolecule could be represented by a multipole expansion, which consists of the superposition of a monopole, dipole, quadrupole, octupole, and so on [23,38]. Mathematically, this means the potential solution of the linearized PBE could be expanded in terms of spherical harmonics. The leading term in the multipole expansion or spherical harmonics expansion is the monopole term. Denote the geometric center of the biomolecule as $\mathbf{r}_c = (x_c, y_c, z_c)$, which can be calculated as

$$\mathbf{r}_c = \frac{1}{N_m} \sum_{i=1}^{N_m} \mathbf{r}_i. \tag{24}$$

The monopole term is actually corresponding to a Kirkwood sphere solution with the total charges of the biomolecule assumed at $\mathbf{r}_c$ and an appropriate radius a [23]

$$u(\mathbf{r}) = \frac{e_c^2}{k_B T} \frac{q e^{\lambda(a - |\mathbf{r} - \mathbf{r}_c|)}}{\epsilon^+(\lambda a + 1)|\mathbf{r} - \mathbf{r}_c|}, \quad \text{for } |\mathbf{r} - \mathbf{r}_c| \geq a, \tag{25}$$

where $q = \sum_{i=1}^{N_m} q_i$. For a boundary node $\mathbf{r} \in \partial\Omega$, define the radial distance from the center of the biomolecule as $r = |\mathbf{r} - \mathbf{r}_c|$. As pointed out in [5], the dipole and quadrupole terms in the multipole expansion will have a decaying factor r^{-2} and r^{-3}, respectively. Thus, when r is sufficiently large, which is the case for a large protein system, the monopole term will dominate other terms, so that Eq. (25) provides a good approximation to the PBE potential at the boundary point $\mathbf{r} \in \partial\Omega$.

With $r = |\mathbf{r} - \mathbf{r}_c|$, the monopole term (25) obviously takes the asymptotic solution form Eq. (20) underlying the RBC derivation. Thus, by taking a directional derivative along the direction $\mathbf{r} - \mathbf{r}_c$ and denoting such a derivative as $\frac{\partial u}{\partial r}$, we propose a ray-casting Robin boundary condition (RBC) for the PB model in 3D

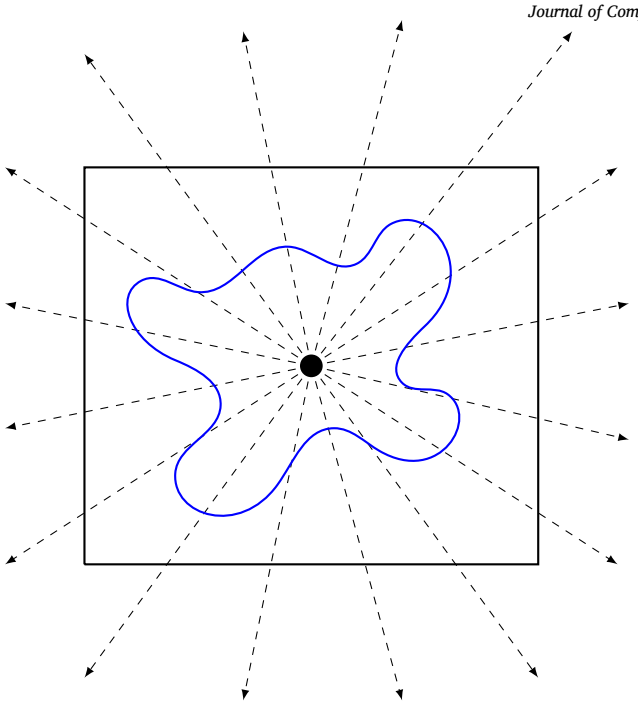

Fig. 6. A 2D illustration of the 3D ray-casting directions involved in the proposed Robin boundary condition Eq. (26).

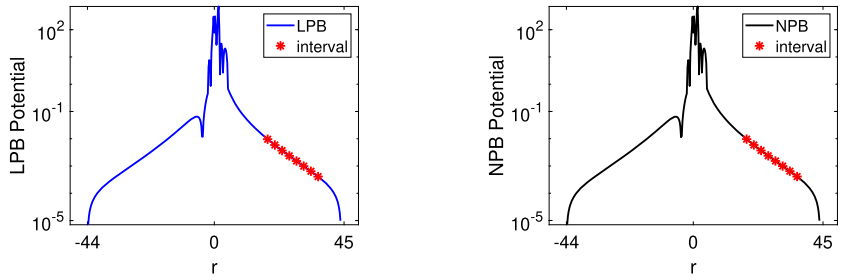

(a) LPB Electrostatic Potential (b) NPB Electrostatic Potential

Fig. 7. The 3D LPB and NPB potentials are converted to 1D arrays along the x-direction. The plots are for the domain $[-44,44]*[-45,45]*[-42,43]$ with a mesh size of $h=0.25$ Å. The red region represents the interval where the asymptotic analysis will be conducted in the x direction.

$$\frac{\partial u}{\partial r}+\left(\frac{1}{r}+\lambda\right)u(\mathbf{r})=0,\quad \text{for } \mathbf{r}\in\partial\Omega. \tag{26}$$

The geometric center and the ray-casting direction $\mathbf{r}-\mathbf{r}_c$ are illustrated in Fig. 6. Note that the actual radius of the monopole term, i.e., a in (25), is not required in our boundary treatment. Basically, a has been absorbed into the asymptotic constant in Eq. (20), and thus can be eliminated. Nevertheless, for the global asymptotic boundary conditions in [5,35], a good estimate of a or the asymptotic constant is indispensable.

4.2. Asymptotic validation of the RBC in 3D

Similar to the 1D studies, we next conduct an asymptotic analysis for the RBC Eq. (26) in 3D. To this end, we numerically solve the 3D PBE Eq. (1) with a Dirichlet zero boundary condition over a finite domain Ω, by using the rMIB package [18]. A small compound *nnd* with 26 atoms is examined, and its geometric center has been translated to the origin, i.e., $\mathbf{r}_c=(0,0,0)$. Because the molecule has a small size, we can test several medium size edge values for generating the domain Ω. For both linear and nonlinear PB models, we take $\epsilon^-=1$, $\epsilon^+=80$, and $I=0.15$. By using $h=0.25$ Å, a numerical potential $u(\mathbf{r})$ is obtained for each case, from which a 1D array will be extracted along the x axis. Like in 1D, we have to choose an appropriate interval for the asymptotic analysis, which should be outside the solute with decaying solution and should not be affected by the boundary pollution. An illustration of a selected interval in x direction is shown in Fig. 7. Similar studies have been conducted for y and z directions as well, and the numerical results are similar and will be omitted here.

Table 2
Asymptotic analysis for 3D LPB and NPB potentials for the small compound *nnd* with $h = 0.25$ Å and different domains. For each case, a 1D potential array is extracted along the x axis for the LS fitting.

	LPB			NPB		
Domain	$\ln K$	α	β	$\ln K$	α	β
$[-29,29]\times[-30,30]\times[-27,28]$	1.297846	0.176826	-0.932305	1.294958	0.176855	-0.931088
$[-34,34]\times[-35,35]\times[-32,33]$	0.954683	0.151805	-0.957865	0.951547	0.151834	-0.956552
$[-44,44]\times[-45,45]\times[-42,43]$	0.862828	0.140146	-1.002597	0.860062	0.140163	-1.001480
$[-52,52]\times[-53,53]\times[-50,51]$	0.680985	0.134753	-0.988875	0.678189	0.134768	-0.987775

With the 1D potential array along the x direction, we conduct the LS fitting to the asymptotic solution given in Eq. (21) for estimating $\ln K$, α and β. The numerical results are reported in Table 2 for both linear and nonlinear potentials over different 3D domains. Asymptotically, it is expected that $\alpha \to \lambda = 0.12572533646057585$ Å^{-1} and $\beta \to -1$ when the edge value goes to infinity and h approaches zero. It can be observed from Table 2 that α indeed converges to λ as the domain becomes larger, while β becomes close to -1. The convergence pattern is not as evident as in Table 1, because very large domain sizes can be used in the 1D analysis, while the domain size is limited to be small to medium for 3D simulations. Given this limitation, the convergence pattern in Table 2 is already very good for the present non-symmetric Cartesian domains. Moreover, one can see that the asymptotic values of LPB and NPB are very similar in Table 2 - suggesting that the NPB potential satisfies the same asymptotic solution as the LPB near the boundary. Finally, we note that the asymptotic analysis is conducted over an interval quite close to the solute region, see Fig. 7. Theoretically, the proposed RBC condition can be applied at any point in this interval. This means that the RBC condition will be valid for a small edge value, which implies a large saving in 3D computations.

4.3. Numerical implementation of the RBC in 3D

A second order finite difference discretization of the modified Robin boundary condition Eq. (26) will be constructed by using the matched interface and boundary (MIB) scheme [12,47], and will be implemented in the rMIB package [18]. In the rMIB PB solver, a uniform mesh is employed with the spacing h being the same in all Cartesian directions, i.e., $h = \Delta x = \Delta y = \Delta z$, while the number of grid nodes is n_x, n_y, and n_z, respectively, in x, y, and z directions. For a grid node (x_i, y_j, z_k), let us denote $u_{i,j,k} = u(x_i, y_j, z_k)$.

A second order central difference is employed to discretize the derivatives in the PBE Eq. (1). For example, away from the interface and boundary, the x derivative at a node (x_i, y_j, z_k) can be approximated as

$$\left[\frac{\partial^2 u}{\partial x^2}\right]_{i,j,k} = \frac{u_{i-1,j,k} - 2u_{i,j,k} + u_{i+1,j,k}}{h^2} + O(h^2). \tag{27}$$

To avoid order reduction, the central difference approximation has to be corrected near the interface Γ and boundary $\partial\Omega$ [47]. For the dielectric interface, a second order accurate MIB scheme [9,17,18,43] has been developed to enforce jump conditions and to accommodate geometrically complex molecular surface in solving the PBE.

The MIB boundary treatment developed in [12] will be reformulated to impose the modified Robin condition Eq. (26) on $\partial\Omega$. In particular, consider a boundary node, such as (x_n, y_j, z_k), where we have denoted $n = n_x$ for simplicity. At this point, the central difference Eq. (27) will be modified as

$$\left[\frac{\partial^2 u}{\partial x^2}\right]_{n,j,k} = \frac{u_{n-1,j,k} - 2u_{n,j,k} + \hat{u}_{n+1,j,k}}{h^2} + O(h^2), \tag{28}$$

where $\hat{u}_{n+1,j,k} = \hat{u}(x_{n+1}, y_j, z_k)$ is a fictitious value outside the domain. If this fictitious value can be estimated accurately, finite difference approximation Eq. (28) maintains a second order of accuracy.

A second order ray-casting MIB scheme is developed to represent $\hat{u}_{n+1,j,k}$. To this end, we first define the geometric center $\mathbf{r}_c = (x_c, y_c, z_c)$ according to Eq. (24). Then a radial direction can be defined by drawing a line from $\mathbf{r}_c$ to the fictitious point (FP) (x_{n+1}, y_j, z_k). See Fig. 6 for an illustration of several ray-casting directions for multiple FPs. The ray-casting line for the FP (x_{n+1}, y_j, z_k) will intersect two yz-planes $x = x_n$ and $x = x_{n-1}$, respectively, at two auxiliary points (APs) $\gamma_1 = (x_n, y_{\gamma_1}, z_{\gamma_1})$ and $\gamma_2 = (x_{n-1}, y_{\gamma_2}, z_{\gamma_2})$, as illustrated in Fig. 8a. A second order finite difference discretization of the Robin condition Eq. (26) will be enforced at the AP $\gamma_1 \in \partial\Omega$ along the radial direction. This gives rise to

$$\frac{\hat{u}(x_{n+1}, y_j, z_k) - u(x_{n-1}, y_{\gamma_2}, z_{\gamma_2})}{r_{n+1} - r_{n-1}} + \left(\frac{1}{r_n} + \lambda\right) u(x_n, y_{\gamma_1}, z_{\gamma_1}) = 0, \tag{29}$$

where $r_{n+1} = \sqrt{(x_{n+1} - x_c)^2 + (y_j - y_c)^2 + (z_k - z_c)^2}$, $r_n = \sqrt{(x_n - x_c)^2 + (y_{\gamma_1} - y_c)^2 + (z_{\gamma_1} - z_c)^2}$, and $r_{n-1} = \sqrt{(x_{n-1} - x_c)^2 + (y_{\gamma_2} - y_c)^2 + (z_{\gamma_2} - z_c)^2}$. From Eq. (29), the fictitious value $\hat{u}$ can be solved in terms of two u values

$$\hat{u}(x_{n+1}, y_j, z_k) = u(x_{n-1}, y_{\gamma_2}, z_{\gamma_2}) - (r_{n+1} - r_{n-1})\left(\frac{1}{r_n} + \lambda\right) u(x_n, y_{\gamma_1}, z_{\gamma_1}). \tag{30}$$

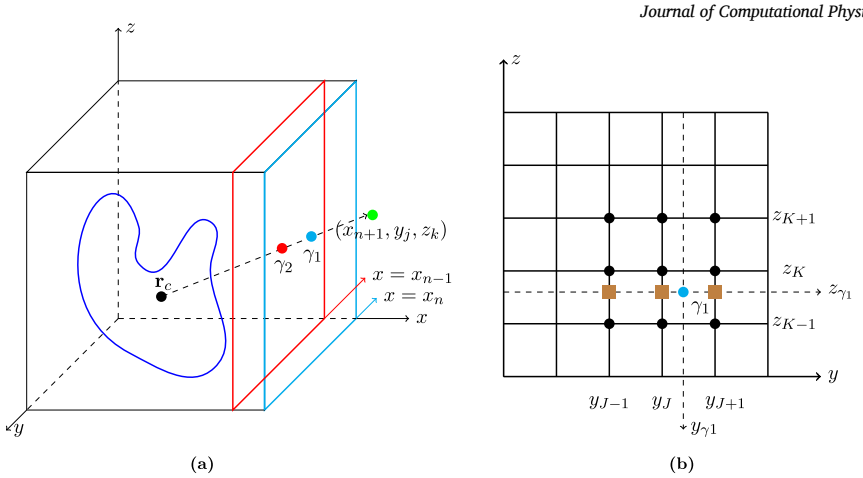

Fig. 8. (a) A 3D illustration of the ray-casting MIB scheme (radial direction) for a fictitious point (FP) (x_{n+1}, y_j, z_k). A radial line is drawn from the center of the solute molecule ($\mathbf{r}_c = (x_c, y_c, z_c)$) to this FP. This radial line intersects the yz-planes $x = x_n$ and $x = x_{n-1}$ at $\gamma_1 = (x_n, y_{\gamma_1}, z_{\gamma_1})$ and $\gamma_2 = (x_{n-1}, y_{\gamma_2}, z_{\gamma_2})$, respectively. The modified Robin boundary condition is discretized at γ_1, which involves points: γ_1, γ_2 and the FP. (b) Since γ_1 and γ_2 are not grid nodes, they will be interpolated in the yz-plane. For example, $\gamma_1 = (x_n, y_{\gamma_1}, z_{\gamma_1})$ will be first interpolated in y direction using three nearest points (brown squares). Then each of the three points will be interpolated in z direction by using three nearest nodes (black circles). Thus, each of γ_1 and γ_2 is interpolated by 9 grid nodes.

We note that two APs $\gamma_1 = (x_n, y_{\gamma_1}, z_{\gamma_1})$ and $\gamma_2 = (x_{n-1}, y_{\gamma_2}, z_{\gamma_2})$ usually are not grid nodes. Thus, the u values at two APs need to be interpolated in the yz-planes. As shown in Fig. 8b, the AP γ_1 will be interpolated along y and z directions, respectively, by using three nearest grid nodes. This involves nine grid nodes in the yz-plane $x = x_n$ to interpolate γ_1, and γ_2 will be treated similarly. The 1D interpolation weights involved in this process are generated by the subroutine given in [14]. By interpolating each AP by nine grid nodes, the fictitious value $\hat{u}(x_{n+1}, y_j, z_k)$ can be expressed as a linear combination of 18 nearby function values

$$\hat{u}(x_{n+1}, y_j, z_k) = \sum_{(x_I, y_J, z_K) \in \mathbb{S}} W_{I,J,K} u(x_I, y_J, z_K), \tag{31}$$

where the set $\mathbb{S}$ contains the aforementioned 18 grid nodes in Ω and the linear combination weights $W_{I,J,K}$ can be computed based on interpolation weights and Eq. (30). Finally, Eq. (31) can be substituted into Eq. (28) to discretize the x derivative in the PBE at this boundary point. The PBE discretization and enforcement of Robin boundary conditions in y and z can be formulated similarly.

5. Numerical validation

In this section, we will examine the accuracy, robustness, and efficiency of the proposed Robin boundary condition (RBC) Eq. (26) and the ray-casting MIB scheme for 3D PB computations. The calculated potential and electrostatic free energy will be benchmarked with the analytical or reference values, and compared with those generated by commonly used boundary conditions, including the Dirichlet zero boundary condition (DBC0) Eq. (4), the Debye-Hückel Dirichlet boundary condition (DBC) Eq. (5), and analytical boundary condition for the Kirkwood sphere (ABC) Eq. (7). All boundary conditions are implemented in the same 3D rMIB PB solver [18]. In all computations, the electrostatic free energy has unit $kcal/mol$, the ionic strength is 0.15, $\epsilon^- = 1$ and $\epsilon^+ = 80$. Unless specified otherwise, the unit of the length of spacing h, domain size and edge value is Å.

5.1. 3D Kirkwood sphere with a centered charge

We first consider a Kirkwood sphere with a central charge $q = 1$ located at the origin $\mathbf{r}_c = (0, 0, 0)$ and radius $a = 2$ Å. A cubic domain $[-b, b]^3$ is employed. For the linearized PB (LPB) model, the analytical potential is available [18], and the analytical electrostatic free energy is $E = -82.188683337726175\ kcal/mol$.

We first explore the impact of the domain size b on the energy calculation in the LPB model. By considering different b values, the energy errors are plotted in Fig. 9a for three boundary conditions. It can be seen that the energies for ABC and RBC produced lower numerical errors regardless of the domain size while the DBC0 required domains larger than $[-20, 20]^3$.

We next examine the potential approximation error of the LPB model, for which the potential u is analytically known for the Kirkwood sphere. By using a domain of $[-6, 6]^3$, numerical errors in L_2 and L_∞ norms are depicted in Fig. 9b and 9c. With a small domain size $b = 6$, the DBC0 condition fails to converge and its error remains as a constant for different h values. The errors of ABC and RBC conditions become smaller as h goes to zero, while the ABC convergence is better because it is derived based on the analytical solution. The LS fitted numerical orders in L_2 and L_∞ norms are found to be: ABC: 2.09 and 2.03, RBC: 1.27 and 1.96 and DBC0: −0.01 and 0.00. In the previous Kirkwood sphere test [18], the ABC is used and the rMIB package has been shown to provide second order accurate potential value for the LPB model [18]. In this work, we found the RBC can also provide second order accurate potential in terms of L_∞ error. The L_2 order of the RBC is slightly less than two, but this does not affect its energy accuracy which is second order accurate.

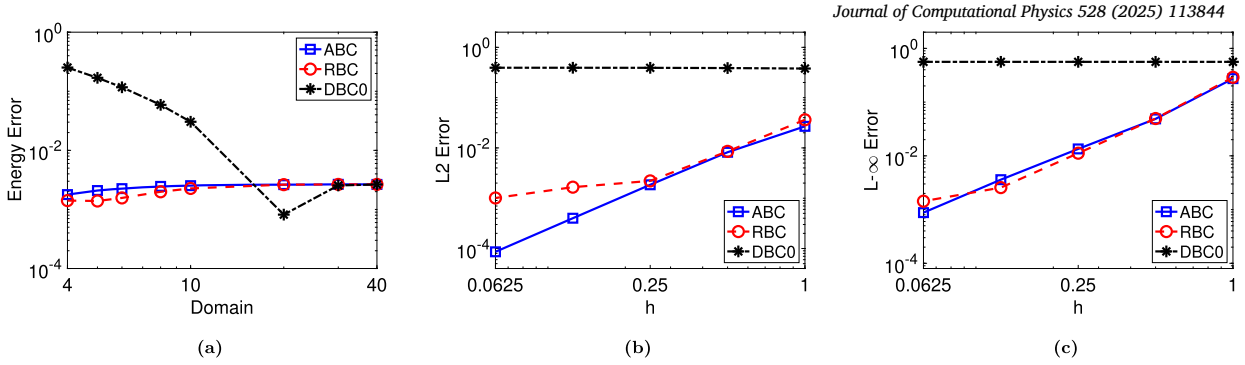

Fig. 9. Numerical approximation of the 3D LPB energy for the Kirkwood sphere ($a = 2$ Å, $q = 1$). (a) Energy error for different domain size b with a fixed $h = 0.25$. (b) L_2 error and (c) L_∞ error in approximating the electrostatic potential by using different h and a fixed domain $[-6, 6]^3$.

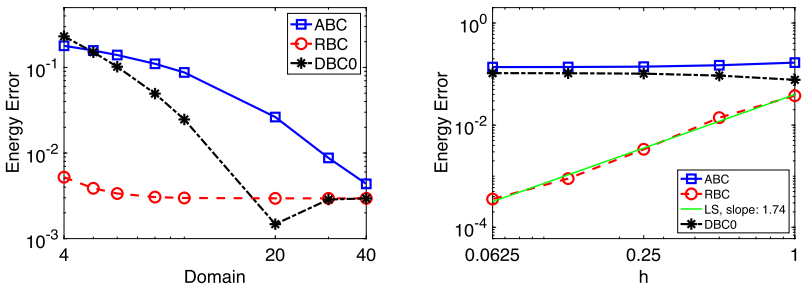

Fig. 10. Numerical error in approximating the 3D NPB energy for the Kirkwood sphere ($a = 2$ Å, $q = 1$). Left: Different domain size b with a fixed $h = 0.25$; Right: Different spacing h with a fixed domain size $b = 6$.

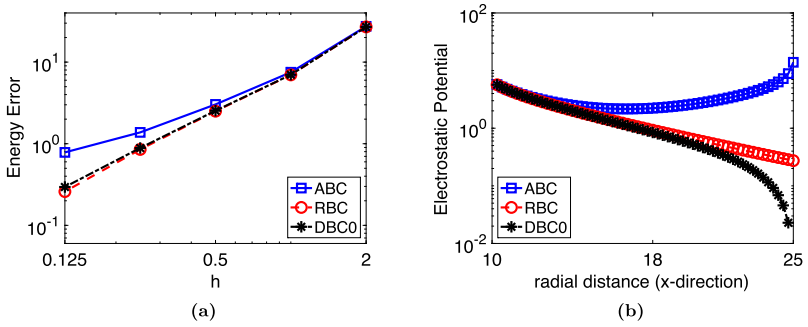

Fig. 11. Energy error and potential of the highly charged Kirkwood sphere with $q = 50$ and $a = 10$ Å. (a) NPB energy error with a fixed domain $b = 25$; (b) The line plot of the NPB potential u along the x-axis with $b = 25$ and $h = 0.25$ in the log scale.

We next study the same Kirkwood sphere with the nonlinear PB (NPB) model, whose reference energy $E = -82.212210265417710\ kcal/mol$ is calculated by using the program developed in [1]. In Fig. 10, the dependencies of the NPB energy error on the domain size b and spacing h are plotted for three boundary conditions. It is obvious that the ABC is the worst boundary condition now, because the ABC condition is derived based on the LPB analytical solution. Compared with the LPB case, the DBC0 condition performs the same. It needs a large domain size, and fails to converge with respect to h when $b = 6$. The RBC condition performs as good as in the linear case by producing a small error for all domain sizes. In Fig. 10 right chart, the LS fitted line of the RBC condition is also plotted, which shows that the energy convergence order is 1.74. This indicates that the proposed RBC together with the ray-casting scheme achieves a second order of convergence in estimating the electrostatic free energy.

Similar to the 1D studies, we also consider a highly charged Kirkwood sphere with a centered charge $q = 50$ and radius $a = 10$ Å. For the nonlinear case, a reference energy $E = -41413.479350115194\ kcal/mol$ is generated by using the 1D solver developed in [1].

We test the energy convergence in Fig. 11a for the NPB model, by using a fixed domain $[-25, 25]^3$ or $b = 25$. The ABC invokes a larger error than the RBC and DBC0. The DBC0 energy converges in the highly charged Kirkwood sphere case, perhaps because the domain size $b = 25$ is large enough. In Fig. 11b, the logarithm of the potential is plotted along the x-axis with $y = z = 0$ for the NPB model. The DBC0 potential obviously attains the boundary value $u = 0$ at $x = 25$. Also, it is clear that the RBC potential still yields a reasonable decaying potential while the ABC potential generates an unphysical solution for the highly charged Kirkwood sphere, where the potential u grows near the boundary.

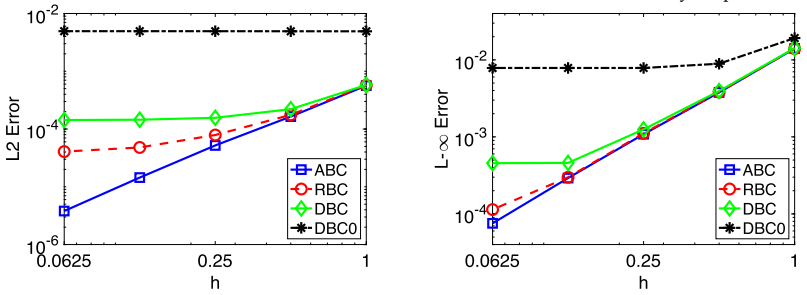

Fig. 12. Numerical accuracy in approximating electrostatic potential of the 3D LPB equation for the Kirkwood sphere of radius $a = 2$ Å with six off-centered charges. A fixed domain $[-6, 6]^3$ is employed. Left: L_2 error; Right: L_∞ error.

Table 3
Numerical errors and orders in approximating the LPB energy for the 3D Kirkwood sphere of radius $a = 2$ Å with six off-centered charges using four boundary conditions. A fixed domain $[-6, 6]^3$ is used.

	ABC			RBC		
h	E	error	order	E	error	order
1	-4105.6616	1.02E+1		-4105.5788	1.02E+1	
1/2	-4098.5704	3.14E+0	1.70	-4098.6164	3.19E+0	1.67
1/4	-4096.3317	9.05E-1	1.80	-4096.3749	9.49E-1	1.75
1/8	-4095.6669	2.41E-1	1.91	-4095.6891	2.63E-1	1.85
1/16	-4095.4886	6.24E-2	1.95	-4095.4979	7.16E-2	1.88
	DBC			DBC0		
h	E	error	order	E	error	order
1	-4105.8199	1.04E+1		-4111.5583	1.61E+1	
1/2	-4098.7280	3.30E+0	1.65	-4104.4433	9.02E+0	0.84
1/4	-4096.4890	1.06E+0	1.64	-4102.1984	6.77E+0	0.41
1/8	-4095.8242	3.98E-1	1.42	-4101.5321	6.11E+0	0.15
1/16	-4095.6459	2.20E-1	0.86	-4101.3530	5.93E+0	0.04

5.2. 3D Kirkwood sphere with off-centered charges

In this subsection, we consider Kirkwood spheres with off-centered charges. In our first test, six charges $(\frac{1}{2}, 1, 2, \frac{1}{2}, 1, 2)$ are considered, which are located at $(1, 0, 0)$, $(-\frac{1}{2}, 0, 0)$, $(0, -\frac{1}{2}, 0)$, $(0, 1, 0)$, $(0, 0, -\frac{1}{2})$ and $(0, 0, 1)$, respectively, in a spherical cavity with radius $a = 2$ Å. Note that the center of charges $\mathbf{r}_c = (\frac{1}{12}, \frac{1}{12}, \frac{1}{12})$ is not located at the origin. Moreover, the charge distribution breaks the spherical symmetry. Thus, such a Kirkwood sphere is a good example for testing the performance of the proposed RBC condition (26) for treating the non-symmetric problem.

In the case of the LPB model, the analytical potential of the Kirkwood sphere with off-centered charges can be calculated by using spherical harmonic expansions [15,17]. Based on that, the analytical energy can be calculated as $E = -4095.4262228752582$ kcal/mol for the present test case. In this subsection, the ABC condition will refer to the Dirichlet boundary condition derived from the analytical potential. Moreover, the commonly used Dirichlet boundary condition (DBC) given in Eq. (5) will also be considered, together with the Dirichlet zero boundary condition (DBC0) Eq. (4).

With the analytical potential in the LPB model, we first test the L_2 and L_∞ convergence in approximating the potential u with successive mesh refinements. By using a fixed domain $[-6, 6]^3$, the numerical results of four boundary conditions are shown in Fig. 12. By using the LS fitting, the rates of convergence in the L_2 and L_∞ norms for four boundary conditions are in order: ABC: 1.72 and 1.85, RBC: 1.43 and 1.83, DBC: 0.94 and 1.75 and, DBC0: −0.00 and 0.64. As before, the DBC0 condition is invalid for a small domain size $b = 6$. The ABC condition exhibits a constant convergence rate, which actually shows the second order of accuracy of the rMIB algorithm [18] for the Kirkwood sphere with multiple charges. Both the RBC and DBC conditions attain converged results, while the convergence rate of the RBC is better and closer to two.

The numerical energies calculated by four boundary conditions are listed in Table 3. By using the analytical energy, the numerical errors are also reported for successive mesh refinements, which allow us to calculate the numerical orders for energy approximation. It can be seen that the DBC0 energy does not converge. The DBC energy is converging, but is very slow. Both ABC and RBC energies attain the second order of convergence.

Next, we extend our analysis to the NPB model for the Kirkwood sphere with multiple charges. We note that no analytical solution exists for the NPB model. Moreover, the 1D NPB energy benchmark program developed in [1] is not applicable, because the present Kirkwood sphere with off-centered charges cannot be reduced to 1D. To compare four boundary conditions, we will mainly examine the electrostatic free energy.

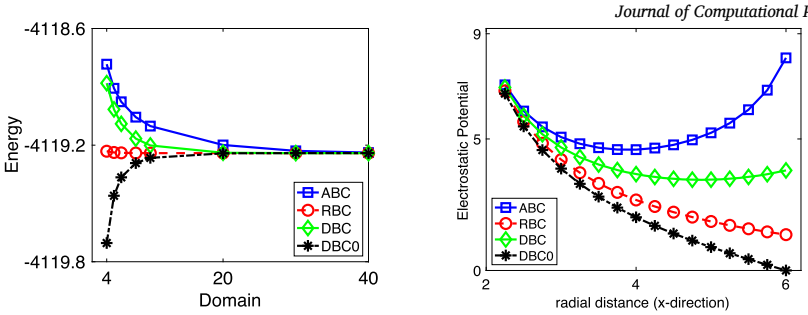

Fig. 13. Numerical solution of the 3D NPB equation for the Kirkwood sphere of radius $a = 2$ Å with six off-centered charges. Left: electrostatic free energies produced by four boundary conditions for different b with $h = 0.25$; Right: the line plot of the potential along x-axis by using a fixed domain $[-6, 6]^3$ and $h = 0.25$.

Table 4
Numerical errors and orders in approximating the NPB energy for the 3D Kirkwood sphere of radius $a = 2$ Å with six off-centered charges using four boundary conditions. A fixed domain $[-6, 6]^3$ is used.

	ABC			RBC		
h	E	error	order	E	error	order
1	-4124.7380	5.72E+0		-4125.1536	6.14E+0	
1/2	-4120.2414	1.23E+0	2.22	-4120.5320	1.52E+0	2.02
1/4	-4118.9770	3.65E-2	5.07	-4119.2399	2.26E-1	2.75
1/8	-4118.7475	2.66E-1	-2.86	-4119.0075	6.02E-3	5.23
1/16	-4118.7523	2.61E-1	0.03	-4119.0125	1.02E-3	2.56
	DBC			DBC0		
h	E	error	order	E	error	order
1	-4124.9299	5.92E+0		-4125.3831	6.37E+0	
1/2	-4120.3687	1.36E+0	2.13	-4120.6777	1.66E+0	1.94
1/4	-4119.0905	7.70E-2	4.14	-4119.3657	3.52E-1	2.24
1/8	-4118.8591	1.54E-1	-1.00	-4119.1294	1.16E-1	1.60
1/16	-4118.8637	1.50E-1	0.04	-4119.1335	1.20E-1	-0.05

By using $h = 0.25$, the electrostatic free energies calculated by four boundary conditions are plotted against the domain size b in Fig. 13 Left. It is obvious that the RBC energy attains the fastest convergence rate - it looks like a constant for all domain sizes. All other energies converge to that of the RBC, but a larger domain size is required. The ABC condition performs the worst, while the convergence rates of the DBC and DBC0 look similar. On the right chart of Fig. 13, the potential u is plotted along the x-axis for four boundary conditions, by using $b = 6$ and $h = 0.25$. We note that the RBC potential is the only correct one. The DBC0 potential artificially equals zero at $x = 6$ as forced by the boundary condition. Both the ABC and DBC potentials are unphysical. They are growing as approaching the boundary and assume local minimals in the solvent domain. Based on Fig. 13 Left Chart, such artifacts could be avoided only when a very large domain size b is used for the ABC and DBC conditions, which, unfortunately, are computationally more expensive.

To quantitatively verify the convergence, a reference energy is needed for the NPB model. Based on the best performance of the RBC condition in Fig. 13, we use the RBC condition with $b = 10$ and $h = 0.0625$ to calculate a reference energy $E = -4119.0135004213835\ kcal/mol$. Based on it, the energy errors of the four boundary conditions are reported in Table 4. The RBC condition produces the smallest errors and the numerical convergence rates are consistently second order or even higher. For the other three conditions, second orders are displayed for large h values, but eventually, the order is down to zero at $h = 1/16$. In fact, comparing the energies at $h = 1/8$ and $h = 1/16$, all conditions yield self-converged results, namely the difference between these two energies is usually less than 5.0E-3. However, with $b = 6$, as shown in Fig. 13 Right, only the RBC condition produces physically correct potentials. The potentials of the other three conditions are actually incorrect. Due to such boundary errors, the energies of these three conditions converge to something different from that of the RBC. This is essentially why the convergence orders of the three conditions become zero at $h = 1/16$, when they are benchmarked with the RBC reference energy.

A Kirkwood sphere with six off-centered high charges is also considered. By taking the radius as $a = 10$ Å, the six off-centered charges are 40, 45, 50, 40, 45 and 50 at positions $(4.5, 0, 0)$, $(-5, 0, 0)$, $(0, -5.0, 0)$, $(0, 4.5, 0)$, $(0, 0, -5)$ and $(0, 0, 4.5)$, respectively. Note that the center of charges $\mathbf{r}_c = (-\frac{1}{12}, -\frac{1}{12}, -\frac{1}{12})$ is also not at the origin.

For simplicity, we only consider the NPB model for the present case. By using $h = 0.25$, the electrostatic free energies calculated by four boundary conditions are plotted against the domain size b in Fig. 14 Left. The RBC energy looks like a constant for all b values, showing the best convergence among the four conditions. For the highly charged case, the ABC condition is the worst and still does not converge with $b = 50$. It is also noted that the commonly used DBC condition is actually worse than the DBC0, because it requires a larger b for energy convergence. By using $b = 25$ and $h = 0.25$, the potentials of four conditions are plotted along the x-axis in Fig. 14 Right. Similar to the previous case, the RBC potential is the only physical one. With a semilogy plot, the RBC potential

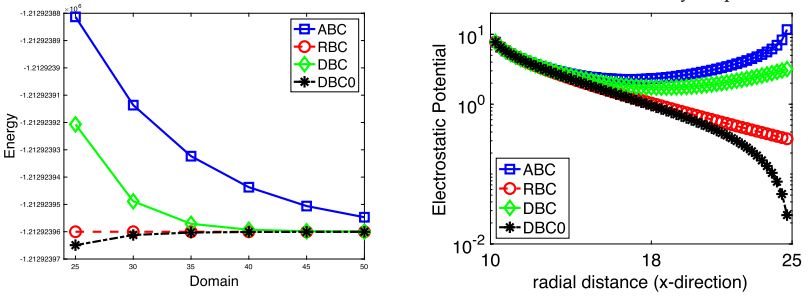

Fig. 14. Numerical solution of the 3D NPB equation for the Kirkwood sphere of radius $a = 10$ Å with six off-centered high charges. Left: electrostatic free energies produced by four boundary conditions for different b with $h = 0.25$; Right: the line plot of the potential along x-axis by using a fixed domain $[-25, 25]^3$ and $h = 0.25$.

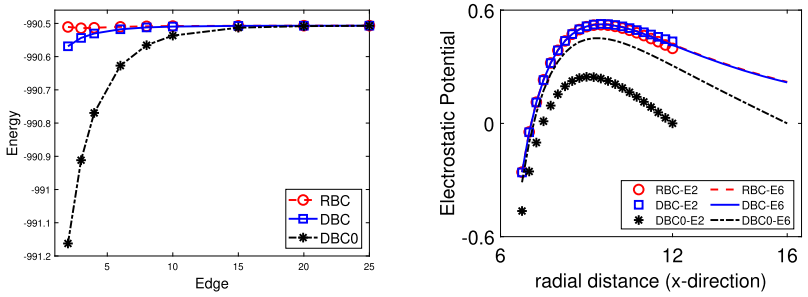

Fig. 15. Numerical solution of the 3D NPB equation for the protein 1bbl. Left: electrostatic free energies produced by three boundary conditions for different edge values with $h = 0.25$; Right: the line plot of the potential along x-axis using edge value 2 (E2) and edge value 6 (E6) with $h = 0.25$.

clearly displays the desired asymptotic pattern. The DBC0 potential was dragged to zero at $b = 25$, so that the decaying pattern was distorted. For the ABC and DBC conditions, the potential is nonphysically increasing as approaching the boundary.

5.3. Electrostatic analysis of a protein

In this subsection, electrostatic analysis will be carried out for a protein with protein databank (PDB) ID: *1bbl*, which has been studied in Ref. [18] by using the rMIB algorithm with the DBC Eq. (5). By using the same package, we will examine two more boundary conditions, i.e., the RBC Eq. (26) and DBC0 Eq. (4). The protein 1bbl has a relatively small size, containing 576 atoms. This allows us to test large edge values and/or dense meshes. For simplicity, we shall focus only on the NPB model for protein studies.

We first explore the impact of the edge value to the electrostatic free energy. By using three boundary conditions, such results are shown in Fig. 15 Left. It is clear the RBC is the best among three conditions. The RBC energy looks like a constant for all edge values and the DBC energy also converges quite fast, while DBC0 requires a large edge value for convergence. An in-depth analysis is conducted in Fig. 15 Right. For each boundary condition, two potential solutions are generated by using edge $= 2$ (E2) and edge $= 6$ (E6) with $h = 0.25$. Then both potential solutions are plotted in the same figure along the x-axis for the solvent domain. It can be observed that when the edge is large enough, such as E6, the potentials of the RBC and DBC are almost identical throughout the solvent domain including at the boundary. Nevertheless, with edge $= 2$ (E2), the potential is slightly different from that of E6 for both RBC and DBC conditions. In particular, the RBC has a little undershooting near the boundary cutoff point, while the DBC has a little overshooting. However, such deviations are very minor so that the potential of E2 still agrees with that of E6 for a majority part of the solvent domain, implying potentials for E2 and E6 are also in good agreement inside the solute domain. Consequently, the energies produced with E2 and E6 should be close to each other. In other words, the energy converges fast with respect to the edge value for both RBC and DBC conditions, which confirms what is observed in Fig. 15 Left. On the other hand, the DBC0 potential has a large deviation from that of RBC and DBC. Moreover, it is significantly different with E2 and E6. As suggested by Fig. 15 Left, only when a very large edge value is used, the DBC0 potential and energy could be close to those of the RBC.

We next study the energy convergence with mesh refinements. A reference energy is generated by the RBC using an edge value of 10 and a grid spacing of 0.125 (dimension of mesh: $= 393 \times 401 \times 385$), which gives $E = -990.65456746840368\ kcal/mol$. By using a small edge value of 3 (domain $= [-22, 13] \times [-16, 20] \times [-18, 16]$), numerical results of three boundary conditions are presented in Table 5. The RBC condition clearly achieves a second order of accuracy in energy calculation, while the DBC0 energy diverges with a small edge value. It is interesting to note that with edge $= 3$, the DBC energy converges to the RBC reference energy, and a second order of convergence is also attained.

Fairly speaking, the DBC condition Eq. (5) performs pretty well in solving the NPB equation for protein simulations. Unlike the previous cases involving the Kirkwood spheres, the DBC condition provides accurate energy estimates and converges in second order even for a small edge value. The physical reasons why the DBC condition works well for protein systems can be justified from two aspects. First, the charges involved in proteins are considered to be low. For example, the total charge of the 1bbl is just 1. The partial

Table 5
Numerical errors and orders in approximating the NPB energy for the protein 1bbl. A fixed edge of 3 or domain = $[-22,13]\times[-16,20]\times[-18,16]$ is used.

	RBC			DBC			DBC0		
h	E	error	order	E	error	order	E	error	order
1	-997.3526	6.70E+0		-997.4115	6.76E+0		-997.7634	7.11E+0	
1/2	-989.6556	9.99E-1	2.75	-989.6903	9.64E-1	2.81	-990.0606	5.94E-1	3.58
1/4	-990.5144	1.40E-1	2.84	-990.5436	1.11E-1	3.12	-990.9117	2.57E-1	1.21
1/8	-990.6640	9.41E-3	3.90	-990.6884	3.39E-2	1.71	-991.0567	4.02E-1	-0.65

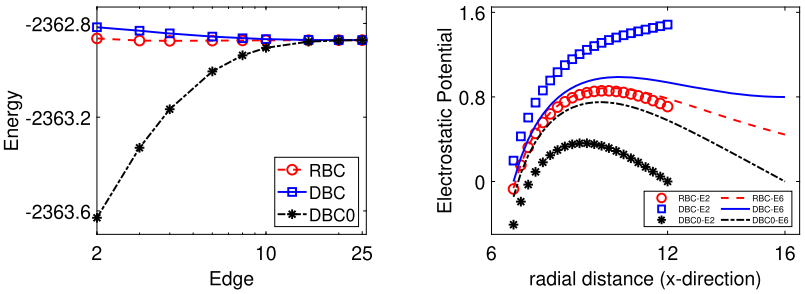

Fig. 16. Numerical solution of the 3D NPB equation for the "highly charged" protein 1bbl. Left: electrostatic free energies produced by three boundary conditions for different edge values with $h = 0.25$; Right: the line plot of the potential along x-axis using edge value 2 (E2) and edge value 6 (E6) with $h = 0.25$.

charge assigned by the force field to each atom center usually has a small magnitude, with a value ranging from $[-0.8, 0.64]$ in case of 1bbl. In other words, q_i in Eq. (5) are all small in magnitude. Second, the domains of protein studies are usually large. For example, with edge = 3, the domain of the 1bbl is $[-22,13]\times[-16,20]\times[-18,16]$. At a boundary point $\mathbf{r}$, most atom centers are far away from it, i.e., $|\mathbf{r}-\mathbf{r}_i|$ is large in Eq. (5). Consequently, the potential value at the boundary will be small and the Debye-Hückel condition calculated by Eq. (5) provides a good approximation to it.

To demonstrate that the DBC condition Eq. (5) could fail for protein studies, we have to artificially create a highly charged test case. To this end, we have chosen three atoms which are close to the right boundary in the x direction, which are atoms *HB1*, *CG* and *HG1* of the Proline amino acid. Their partial charges have been changed from 0.090, -0.180, 0.090 to 3.090, -3.180, 3.090, respectively, for *HB1*, *CG*, *HG1*. The other charges, atom centers and radii are kept the same. The resulting structure will be called as a "highly charged" 1bbl protein.

The above electrostatic analysis is repeated for the "highly charged" 1bbl. The performance of the proposed RBC condition is not affected by the changes. With different edge values, the RBC energy still looks like a constant in Fig. 16 Left. In the right chart, the RBC potentials based on edge = 2 (E2) and edge = 6 (E6) agree pretty well. The DBC0 also behaves similarly as above. It requires a large edge value for energy convergence, and the DBC0 potentials with E2 and E6 are significantly different. The DBC condition is greatly impacted by three high charges artificially created in the 1bbl. Its energy convergence obviously becomes worse in Fig. 16 Left. In potential plots, the DBC potential with edge = 2 becomes unphysical, i.e., it is growing near the boundary. With edge = 6, the DBC potential decays initially, but approaches a constant near the boundary. Moreover, the DBC potentials with E2 and E6 are entirely different throughout the solvent domain. In short, with a few charges changed, the DBC condition exhibits unphysical behaviors near the boundary. Only the RBC condition can correctly capture the asymptotic decaying pattern.

5.4. Electrostatics on a set of proteins

Finally, we conduct the electrostatic analysis for a set of proteins. This set contains 25 proteins, which are randomly chosen from the proteins being studied in [18,46]. The rMIB PB solver [18] will be used to solve the NPB equation with three boundary conditions, DBC Eq. (5), RBC Eq. (26) and DBC0 Eq. (4). By using the default edge value of 3, the electrostatic free energies calculated by using $h = 1$, $h = 0.5$ and $h = 0.25$ are reported in Table 6 for three boundary conditions.

As shown in the above experiments that the proposed RBC condition and the corresponding MIB scheme provide a second order boundary treatment for the NPB model. The RBC energies listed in Table 6 confirm again the second order of convergence. On the other hand, because the partial charges are small and because the protein domain is large, the DBC condition Eq. (5) also provides a good boundary approximation for protein systems. Thus, it can be seen from Table 6 that the DBC and RBC energies converge to the same limit. Moreover, because of the two physical reasons, the DBC0 condition provides a not-bad boundary treatment for protein studies. In Table 6, the DBC0 energy is quite close to those of RBC and DBC.

To visualize the energy convergence, we will treat the RBC energy at $h = 0.25$ as the benchmark for each protein. Then, the difference between the benchmark and the energy calculated by using other conditions and/or different h values is depicted in Fig. 17. From the graph, it can be seen that for $h = 1$ and $h = 0.5$, all boundary conditions have almost the same convergence pattern.

Table 6
Nonlinear PB electrostatic free energies generated by DBC, RBC and DBC0 for a set of 25 proteins for various mesh sizes, using the rMIB PB solver [18].

PDB	DBC			RBC			DBC0		
h	1	0.5	0.25	1	0.5	0.25	1	0.5	0.25
1r69	-1109.95	-1089.98	-1091.78	-1109.87	-1089.95	-1091.76	-1110.25	-1090.29	-1092.09
1sh1	-754.23	-755.79	-756.29	-754.09	-755.69	-756.20	-754.43	-756.03	-756.54
1bbl	-997.41	-989.69	-990.54	-997.35	-989.66	-990.51	-997.76	-990.06	-990.91
1a63	-2414.79	-2379.04	-2382.40	-2414.63	-2378.93	-2382.30	-2415.26	-2379.53	-2382.89
1ajj	-1143.72	-1142.53	-1143.50	-1143.61	-1142.50	-1143.48	-1144.04	-1142.93	-1143.90
2fma	-1061.98	-1043.49	-1044.32	-1061.91	-1043.48	-1044.32	-1062.06	-1043.58	-1044.41
1iua	-958.20	-920.98	-922.58	-958.17	-920.97	-922.59	-958.32	-921.11	-922.71
1vii	-914.22	-904.30	-905.49	-914.13	-904.26	-905.47	-914.53	-904.64	-905.83
1bor	-856.98	-854.63	-856.09	-856.96	-854.63	-856.11	-857.26	-854.92	-856.38
1vb0	-939.00	-896.50	-898.49	-938.99	-896.50	-898.50	-939.02	-896.54	-898.53
1zuu	-1280.52	-1251.96	-1253.37	-1280.64	-1252.11	-1253.57	-1280.86	-1252.30	-1253.72
2erl	-967.32	-953.33	-954.05	-966.98	-953.43	-954.19	-967.87	-953.89	-954.60
1neq	-1765.16	-1734.85	-1737.89	-1765.10	-1734.86	-1737.92	-1765.65	-1735.40	-1738.44
1a2s	-1932.07	-1923.44	-1925.00	-1932.04	-1923.46	-1925.06	-1932.72	-1924.11	-1925.68
1x8q	-2527.01	-2459.51	-2463.80	-2527.01	-2459.51	-2463.81	-2527.11	-2459.64	-2463.93
2h5c	-1920.57	-1827.75	-1831.55	-1920.40	-1827.83	-1831.66	-1920.70	-1827.92	-1831.73
1g6x	-1359.84	-1320.87	-1323.06	-1359.51	-1320.95	-1323.17	-1360.04	-1321.10	-1323.29
1hpt	-825.93	-812.35	-815.11	-825.95	-812.36	-815.16	-826.08	-812.49	-815.25
1bpi	-1324.94	-1305.63	-1307.59	-1324.96	-1305.69	-1307.68	-1325.43	-1306.14	-1308.11
1fxd	-3332.38	-3324.43	-3325.43	-3332.39	-3324.69	-3325.73	-3333.86	-3326.02	-3327.03
1cbn	-308.12	-303.53	-304.16	-308.08	-303.54	-304.18	-308.18	-303.60	-304.22
1c75	-1448.86	-1430.19	-1431.59	-1448.87	-1430.38	-1431.82	-1449.13	-1430.53	-1431.94
1nwz	-2066.33	-2024.46	-2027.42	-2066.40	-2024.53	-2027.51	-2066.49	-2024.62	-2027.58
1zzk	-1345.93	-1313.66	-1317.13	-1345.93	-1313.72	-1317.21	-1346.20	-1313.95	-1317.42
2fwh	-1820.22	-1767.70	-1770.79	-1820.24	-1767.78	-1770.89	-1820.34	-1767.87	-1770.96

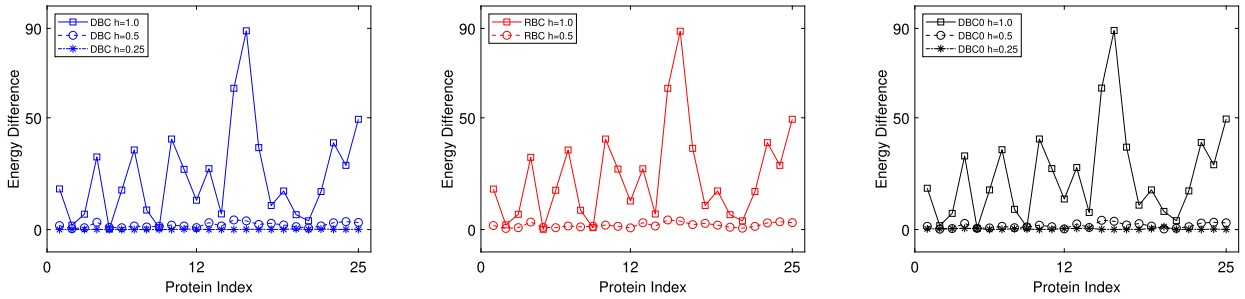

Fig. 17. Energy difference for each boundary condition at different mesh sizes, using the RBC energy at $h = 0.25$ as the benchmark energy: (a) DBC; (b) RBC; (c) DBC0.

At $h = 0.25$, the energy difference of the DBC looks like a constant line with vanishing values, while that of the DBC0 is also quite flat. This indicates that both DBC and DBC0 energies converge to that of the RBC.

We further analyze the computational cost incurred by the DBC and RBC in generating the energies reported in Table 6. Note that a fixed edge of value 3 is employed in all cases. For each protein and each h value, the total spatial degree of freedom $N = n_x \times n_y \times n_z$ is the same for the DBC and RBC. In the rMIB package [18], the linear system $Au = b$ is solved by an iterative solver, i.e., the biconjugate gradient algorithm. The discretization matrix A is the same for interior nodes. At a boundary node, the DBC condition just needs to set a diagonal value one for A, while the RBC condition involves more sparse coefficients in A. For example, as discussed in the ray-casting MIB scheme, each fictitious value will involve 18 coefficients in A. Furthermore, without a fixed boundary value, it is found in our computations that the RBC condition typically requires more iteration numbers than the DBC.

The CPU time of the DBC and RBC for different N is plotted in the log-log scale in Fig. 18a. It can be seen that both conditions have similar computational complexity, while the RBC condition is usually more expensive. By using the LS fitting, the complexity of the DBC and RBC is found to be $O(N^{1.23})$ and $O(N^{1.19})$, respectively. This demonstrates the efficiency of the rMIB inexact Newton algorithm for solving the nonlinear PB equation. In Fig. 18b, the relative CPU difference between the RBC and DBC is plotted against the number of unknowns N. For most simulations, the RBC requires 10% to 90% more CPU time than the DBC. Despite the marginal increase in CPU time, the RBC's overall accuracy and robustness, as demonstrated in the previous experiments, suggest that it remains a highly suitable choice of boundary condition for PB simulations.

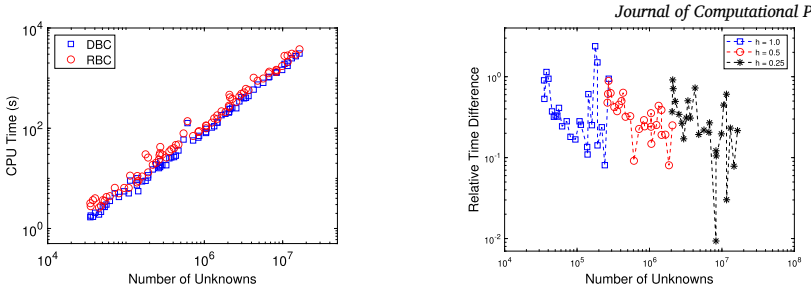

Fig. 18. (a) CPU time (in seconds) for DBC and RBC across all mesh sizes. (b) Relative time difference illustrating the additional time required by RBC across all mesh sizes.

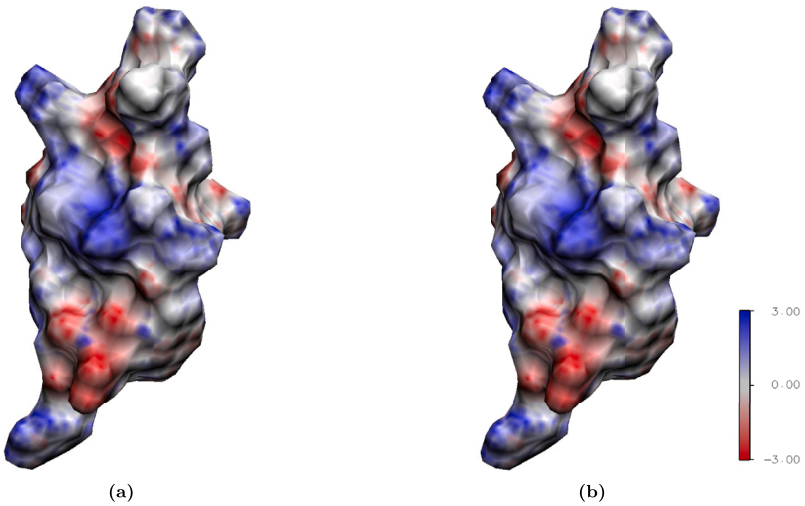

Fig. 19. Electrostatic potential mapped onto the molecular surface for a non-spherical protein (PDB ID: *2nls*). (a) DBC; (b) RBC.

5.5. An extreme case

The proposed Robin condition is derived based on the assumption that the monopole term in the multipole expansion dominates the asymptotic solution near the boundary. Because the monopole term is essentially a Kirkwood sphere solution, concerns could be raised that the accuracy of the RBC may be impaired for proteins with non-spherical shapes. To test this, an extreme case is considered in this subsection.

To validate a new approach for reproducing the ensemble average polar solvation energy, a set of 74 representative proteins has been selected in [8]. The proteins retrieved were required to have at most 30% sequence similarity. A shape analysis of this set of proteins has been conducted in [32] by calculating the ratio of the distance between the two farthest atoms to the radius of gyration. Their findings revealed that protein *2nls* attains the largest ratio. In other words, *2nls* deviates the most from the spherical shape in this set of 74 proteins, making it an ideal candidate for the present study.

By using the NPB model with $h = 0.5$, the electrostatic free energies generated by DBC and RBC are found to be, respectively, −537.6172 and −537.5667. Fig. 19 compares the surface potentials generated by RBC and DBC for the protein *2nls*. First, it is clear that the shape of *2nls* is significantly different from a sphere. Second, there is no visible difference between the colored patterns of the two boundary conditions. This indicates that two boundary conditions not only yield very similar free energies but also produce nearly identical potential distributions. The present study further underscores the robustness and accuracy of the RBC for proteins of any shape.

6. Conclusion

In this paper, we introduced a modified Robin boundary condition (RBC) for the electrostatic analysis of biomolecules in the Poisson-Boltzmann (PB) model. Physically, the boundary condition of the PB model is defined at infinity where the electrostatic potential decays to zero. For grid-based finite difference and finite element methods, a finite domain has to be employed and the corresponding boundary treatment is a known challenge in the numerical solution of the nonlinear PB equation (PBE). Dirichlet boundary conditions [3,20] are usually employed in biomolecular simulations. However, as shown in this work and in [5], Dirichlet conditions could lead to unphysical solutions in many cases. To resolve this issue, some asymptotic boundary conditions have been

developed in the literature [5,30,35]. Nevertheless, these conditions are usually global in nature and have to resort to iterative algorithms for calculating volume integrals from the previous step. Moreover, their complex formulation limits their application in popular PB solvers.

To overcome the aforementioned limitations, a modified Robin condition is derived in this work as a local boundary condition for the nonlinear PBE. The derivation is based on the facts that away from the biomolecule, the asymptotic decaying pattern of the nonlinear PBE is essentially the same as that of the linearized PBE, and the monopole term will dominate other terms in the multipole expansion. Asymptotic analysis has been carried out to validate the application range and robustness of the proposed Robin condition. Moreover, a second order boundary implementation of the proposed RBC by means of a matched interface and boundary (MIB) scheme has been constructed for three-dimensional biomolecular simulations.

By studying Kirkwood spheres with centered charges or off-centered charges and various proteins, the performance of the RBC condition has been extensively validated and compared with the analytical boundary conditions and existing Dirichlet boundary conditions. In all cases, the RBC condition is found to be among the most accurate methods for approximating the electrostatic potential and free energy. Moreover, the RBC condition delivers a second order of convergence in calculating the potential and energy for both linear and nonlinear PBEs, regardless of symmetrical Kirkwood spheres or non-symmetrical biomolecules. Compared with other boundary conditions, the RBC is very robust in two aspects. First, it can produce the correct energy for very small domain sizes or edge values in protein simulations, while the Dirichlet conditions usually require a larger domain. Second, it always produces physically correct solutions in the case of highly charged Kirkwood spheres and proteins, whereas the Dirichlet conditions lead to non-decaying or distorted patterns near the boundary.

For highly charged cases, the Dirichlet boundary condition (DBC) Eq. (5) requires a larger domain to avoid unphysical solutions, while the RBC works for a small domain. Thus, the RBC simulation could be more efficient than the DBC, due to the use of a smaller degree of freedom N. However, for protein simulations, because the partial charges are small and because the domain is large, the DBC Eq. (5) provides a good boundary approximation even with a small edge value. In such a situation, the RBC and DBC computations have a similar complexity, roughly on the order of $O(N^{1.2})$. Nevertheless, the iterative solution in the RBC involves more steps of iterations, so that the RBC is more expensive than the DBC for protein studies. In future studies, we will improve the boundary implementation and explore different iterative algorithms or preconditioning techniques so that the computational efficiency of the RBC could be enhanced.

CRediT authorship contribution statement

Sylvia Amihere: Writing – original draft, Visualization, Validation, Software, Methodology. **Yiming Ren:** Writing – review & editing, Validation, Software. **Weihua Geng:** Writing – review & editing, Software. **Shan Zhao:** Writing – original draft, Supervision, Methodology, Conceptualization.

Funding

Zhao's research is partially supported by the National Science Foundation (NSF) of USA under grants DMS-2110914 and DMS-2306991. Geng's research is partially supported by the NSF under grant DMS-2110922.

Declaration of competing interest

The authors declare that they have no known competing financial interests or personal relationships that could have appeared to influence the work reported in this paper.

Data availability

The protein structures analyzed in this study were downloaded from the protein databank https://www.rcsb.org, and processed according to the cited references.

References

[1] S. Amihere, W. Geng, S. Zhao, Benchmarking electrostatic free energy of the nonlinear Poisson–Boltzmann model for the Kirkwood sphere, Commun. Inf. Syst. 22 (3) (2022) 305–315.
[2] N.A. Baker, Improving implicit solvent simulations: a Poisson-centric view, Curr. Opin. Struct. Biol. 15 (2) (2005) 137–143.
[3] N.A. Baker, D. Sept, M.J. Holst, J.A. Mccammon, The adaptive multilevel finite element solution of the Poisson-Boltzmann equation on massively parallel computers, IBM J. Res. Dev. 45 (3–4) (2001) 427–438.
[4] N.A. Baker, D. Sept, S. Joseph, M.J. Holst, J.A. McCammon, Electrostatics of nanosystems: application to microtubules and the ribosome, Proc. Natl. Acad. Sci. USA 98 (18) (2001) 10037–10041.
[5] A.H. Boschitsch, M.O. Fenley, A new outer boundary formulation and energy corrections for the nonlinear Poisson–Boltzmann equation, J. Comput. Chem. 28 (5) (2007) 909–921.
[6] A.H. Boschitsch, M.O. Fenley, A fast and robust Poisson–Boltzmann solver based on adaptive Cartesian grids, J. Chem. Theory Comput. 7 (5) (2011) 1524–1540.
[7] A.H. Boschitsch, M.O. Fenley, H.-X. Zhou, Fast boundary element method for the linear Poisson-Boltzmann equation, J. Phys. Chem. B 106 (10) (2002) 2741–2754.
[8] A. Chakravorty, Z. Jia, L. Li, S. Zhao, E. Alexov, Reproducing the ensemble average polar solvation energy of a protein from a single structure: Gaussian-based smooth dielectric function for macromolecular modeling, J. Chem. Theory Comput. 14 (2) (2018) 1020–1032.

[9] D. Chen, Z. Chen, C. Chen, W. Geng, G.-W. Wei, Mibpb: a software package for electrostatic analysis, J. Comput. Chem. 32 (4) (2011) 756–770.
[10] R. Chowdhury, R. Egan, D. Bochkov, F. Gibou, Efficient calculation of fully resolved electrostatics around large biomolecules, J. Comput. Phys. 448 (2022) 110718.
[11] V.B. Chu, Y. Bai, J. Lipfert, D. Herschlag, S. Doniach, Evaluation of ion binding to dna duplexes using a size-modified Poisson-Boltzmann theory, Biophys. J. 93 (9) (2007) 3202–3209.
[12] H. Feng, S. Zhao, A fourth order finite difference method for solving elliptic interface problems with the fft acceleration, J. Comput. Phys. 419 (2020) 109677.
[13] F. Fogolari, A. Brigo, H. Molinari, The Poisson–Boltzmann equation for biomolecular electrostatics: a tool for structural biology, J. Mol. Recognit. 15 (6) (2002) 377–392.
[14] B. Fornberg, Classroom note: calculation of weights in finite difference formulas, SIAM Rev. 40 (3) (1998) 685–691.
[15] W. Geng, A boundary integral Poisson-Boltzmann solvers package for solvated bimolecular simulations, Comput. Math. Biophys. 3 (1) (2015).
[16] W. Geng, R. Krasny, A treecode-accelerated boundary integral Poisson-Boltzmann solver for electrostatics of solvated biomolecules, J. Comput. Phys. 247 (2013) 62–78.
[17] W. Geng, S. Yu, G. Wei, Treatment of charge singularities in implicit solvent models, J. Chem. Phys. 127 (11) (2007) 114106.
[18] W. Geng, S. Zhao, A two-component matched interface and boundary (mib) regularization for charge singularity in implicit solvation, J. Comput. Phys. 351 (2017) 25–39.
[19] M. Holst, J.A. McCammon, Z. Yu, Y.C. Zhou, Y. Zhu, Adaptive finite element modeling techniques for the Poisson-Boltzmann equation, Commun. Comput. Phys. 11 (1) (2012) 179–214.
[20] M.J. Holst, The Poisson-Boltzmann Equation: Analysis and Multilevel Numerical Solution, PhD thesis, UIUC, 1994.
[21] M.J. Holst, F. Saied, Numerical solution of the nonlinear Poisson–Boltzmann equation: developing more robust and efficient methods, J. Comput. Chem. 16 (3) (1995) 337–364.
[22] B. Honig, A. Nicholls, Classical electrostatics in biology and chemistry, Science 268 (5214) (1995) 1144–1149.
[23] J.D. Jackson, Classical Electrodynamics, 2nd ed., Wiley, New York, NY, 1975.
[24] A. Lee, W. Geng, S. Zhao, Regularization methods for the Poisson-Boltzmann equation: comparison and accuracy recovery, J. Comput. Phys. 426 (2021) 109958.
[25] B. Lee, F.M. Richards, The interpretation of protein structures: estimation of static accessibility, J. Mol. Biol. 55 (3) (1971) 379–IN4.
[26] C. Li, L. Li, J. Zhang, E. Alexov, Highly efficient and exact method for parallelization of grid-based algorithms and its implementation in delphi, J. Comput. Chem. 33 (24) (2012) 1960–1966.
[27] B. Liu, B. Wang, R. Zhao, Y. Tong, G.-W. Wei, Eses: Software for Eulerian Solvent Excluded Surface, 2017.
[28] B. Lu, X. Cheng, J.A. McCammon, "New-version-fast-multipole-method" accelerated electrostatic calculations in biomolecular systems, J. Comput. Phys. 226 (2) (2007) 1348–1366.
[29] M. Mirzadeh, M. Theillard, A. Helgadottir, D. Boy, F. Gibou, An adaptive, finite difference solver for the nonlinear Poisson-Boltzmann equation with applications to biomolecular computations, Commun. Comput. Phys. 13 (1) (2013) 150–173.
[30] H. Nakamura, S. Nishida, Numerical calculations of electrostatic potentials of protein-solvent systems by the self consistent boundary method, J. Phys. Soc. Jpn. 56 (4) (1987) 1609–1622.
[31] D.D. Nguyen, B. Wang, G.-W. Wei, Accurate, robust, and reliable calculations of Poisson–Boltzmann binding energies, J. Comput. Chem. 38 (13) (2017) 941–948.
[32] S.K. Panday, A. Chakravorty, S. Zhao, E. Alexov, On delivering polar solvation free energy of proteins from energy minimized structures using a regularized super-Gaussian Poisson–Boltzmann model, J. Comput. Chem. 46 (2025) e27496.
[33] Y. Ren, S. Amihere, W. Geng, S. Zhao, Comparison of three matched interface and boundary (mib) schemes for solving the nonlinear Poisson-Boltzmann equation, Commun. Inf. Syst. 24 (2024) 231–251.
[34] F.M. Richards, Areas, volumes, packing, and protein structure, Annu. Rev. Biophys. Bioeng. 6 (1) (1977) 151–176.
[35] W. Rocchia, Poisson-Boltzmann equation boundary conditions for biological applications, Math. Comput. Model. 41 (10) (2005) 1109–1118.
[36] W. Rocchia, E. Alexov, B. Honig, Extending the applicability of the nonlinear Poisson-Boltzmann equation: multiple dielectric constants and multivalent ions, J. Phys. Chem. 105 (2001) 6507–6514.
[37] M.F. Sanner, A.J. Olson, J.-C. Spehner, Reduced surface: an efficient way to compute molecular surfaces, Biopolymers 38 (3) (1996) 305–320.
[38] M.J. Schnieders, N.A. Baker, P. Ren, J.W. Ponder, Polarizable atomic multipole solutes in a Poisson-Boltzmann continuum, J. Chem. Phys. 126 (12) (03 2007) 124114.
[39] Y. Taur, T.H. Ning, Fundamentals of Modern VLSI Devices, Cambridge University Press, 2021.
[40] S.A. Ullah, X. Yang, B. Jones, S. Zhao, W. Geng, G.-W. Wei, Bridging Eulerian and Lagrangian Poisson–Boltzmann solvers by eses, J. Comput. Chem. 45 (6) (2024) 306–320.
[41] L. Wilson, W. Geng, R. Krasny, Tabi-pb 2.0: an improved version of the treecode-accelerated boundary integral Poisson-Boltzmann solver, J. Phys. Chem. B 126 (37) (2022) 7104–7113, PMID: 36101978.
[42] D. Xie, New solution decomposition and minimization schemes for Poisson-Boltzmann equation in calculation of biomolecular electrostatics, J. Comput. Phys. 275 (2014) 294–309.
[43] S. Yu, W. Geng, G.W. Wei, Treatment of geometric singularities in implicit solvent models, J. Chem. Phys. 126 (2007) 244108.
[44] S. Yu, G.W. Wei, Three-dimensional matched interface and boundary (MIB) method for treating geometric singularities, J. Comput. Phys. 227 (2007) 602–632.
[45] B. Zhang, B. Lu, X. Cheng, J. Huang, N.P. Pitsianis, X. Sun, J.A. McCammon, Mathematical and numerical aspects of the adaptive fast multipole Poisson-Boltzmann solver, Commun. Comput. Phys. 13 (1) (2013) 107–128.
[46] S. Zhao, I.E. Ijaodoro, M. McGowan, E. Alexov, Calculation of electrostatic free energy for the nonlinear Poisson-Boltzmann model based on the dimensionless potential, J. Comput. Phys. 497 (2024) 112634.
[47] Y. Zhou, S. Zhao, M. Feig, G.-W. Wei, High order matched interface and boundary method for elliptic equations with discontinuous coefficients and singular sources, J. Comput. Phys. 213 (1) (2006) 1–30.